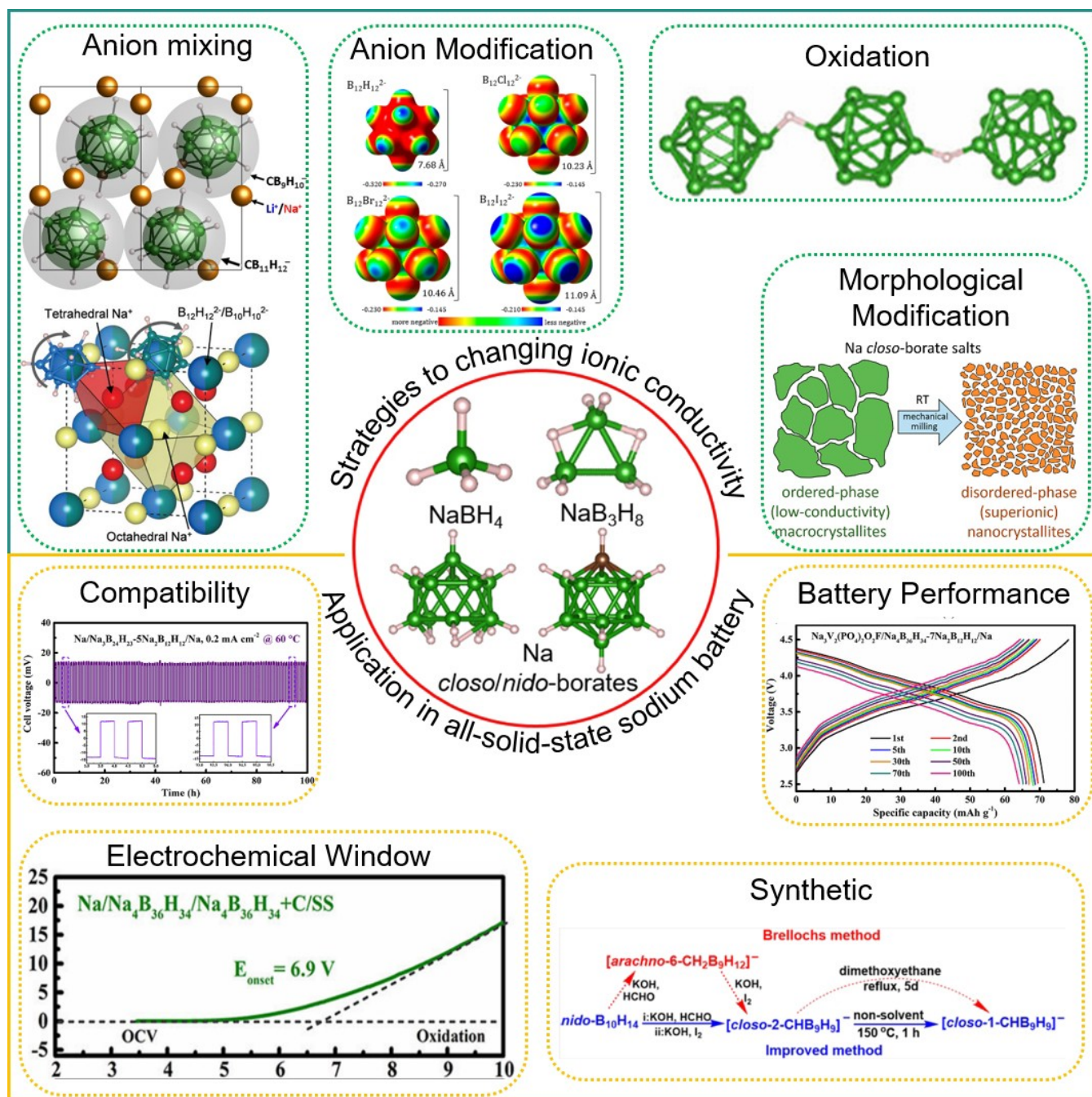


Hydridoborate-Based Solid-State Electrolytes for Sodium Metal Batteries

Zhiwei Lu,^[a] Jia-Xin Kang,^[b] Pengtao Qiu,^{*[b]} and Xuenian Chen^{*[a, b]}



Hydridoborates have emerged as promising candidates for solid-state electrolytes in sodium metal batteries owing to their high ionic conductivity, thermal/electrochemical stability, good mechanical properties, and good interface compatible with electrodes. This review provides a comprehensive analysis of the recent advancements in the development and application of Na-hydridoborate-based solid-state electrolytes. We explore the structural properties and electrochemical behaviors of

various Na-hydridoborates, including NaBH_4 , NaB_3H_8 , *closoborates*, *nido*-borates, etc. Additionally, we discuss the approaches for the synthesis of hydridoborate compounds with inexpensive raw chemicals and low toxicity. This review will inspire further efforts to develop fast Na-ion conducting hydridoborate materials with favorable interfacial compatibility, to promote their applications in high-performance all-solid-state sodium metal batteries.

1. Introduction

The excellent performance of lithium-ion batteries (LIBs) has led to their extensive utilization in electric vehicles and consumer electronic products.^[1] The ever-increasing scale of demand will lead to further price increases due to supply chain vulnerabilities, because lithium resources are limited and concentrated in certain geographic regions.^[2] Therefore, there is a need for alternative, cost-effective energy storage options that do not compromise energy density or efficiency.^[3] Since sodium belongs to the same group as lithium in the periodic table of elements and has abundant terrestrial resources and similar chemical properties, it has gradually attracted more attention from researchers, with the corresponding sodium-ion batteries (NIBs) have been proposed as a complement to lithium-ion batteries.^[4] Additionally, all-solid-state batteries (ASSBs) with solid-state electrolytes (SSEs) have also been extensively researched, due to the potential superiority of safety, polarization, and thermal/electrochemical stability compared to batteries with conventional liquid electrolytes.^[5] The components of ASSBs and the specific requirements for SSEs are shown in Figure 1. Ideal SSEs should combine properties such as high ionic conductivity, thermal stability, transference number, electrochemical stability, environmental friendliness, good mechanical strength, low electronic conductivity, cost-effectiveness, and strong electrode compatibility.^[6] So far, the researchers have shown strong interest in candidate SSEs, with various studies are currently underway to develop all-solid-state sodium metal batteries (ASSMBs), primarily focusing on oxides,^[7] sulfides,^[8] polymers,^[9] halides,^[10] and hydridoborates.^[11] However, achieving the high performance required for SSEs in ASSMBs remains a significant challenge.

Oxide SSEs exhibit high thermal and chemical stability, along with excellent electrochemical oxidation voltage and mechanical strength. Nonetheless, these materials require additional high-temperature (HT) sintering and exhibit stiffness and brittleness, which leads to poor contact with electrodes. This results in complex and expensive manufacturing processes, potentially impeding large-scale production.^[12] Sulfide SSEs offer excellent

ductility and high ionic conductivities ranging from 10^{-2} to 10^{-3} Scm^{-1} at room temperature (RT), even surpassing those of traditional liquid electrolytes. However, they face challenges such as limited chemical stability with electrodes, a narrow electrochemical window, and potential decomposition with H_2S release under ambient conditions, among other.^[13] While polymer electrolytes have enabled significant device integration, they are not yet competitive with other SSEs in terms of energy density, high transference number, and thermal stability.^[14] Halide SSEs exhibit exceptional electrochemical stability, compatibility with high-voltage cathode materials, and RT ionic conductivities of up to 10^{-3} Scm^{-1} . However, they suffer from inadequate stability with bare metals or metal alloys due to high reduction potentials and poor storage stability caused by moisture sensitivity.^[10,15] Hydridoborates have emerged as promising candidates for SSE applications due to their high ionic conductivities (up to 10^{-2} Scm^{-1} and nearly 10^{-1} Scm^{-1}) and durability under high voltage.^[16] Additionally, their unique structures and electronic networks endow hydridoborates with several exceptional properties, including a wide operating potential window, high electrochemical stability, excellent compatibility with both cathodes and anodes, and a low density (20% to 55% lower than that of oxides and sulfides).^[16c] However, the high cost of hydridoborates is a significant drawback limiting the application.

Research on hydridoborates as SSEs dates back to the 1970s, with studies on $\text{Li}_2\text{B}_{10}\text{Cl}_{10}$ and $\text{Li}_2\text{B}_{12}\text{Cl}_{12}$.^[17] However, only a few reports on hydridoborate SSEs followed until 2007, when Orimo et al. observed a significant increase in the ionic conductivity of LiBH_4 after a phase transition.^[18] This pioneering work reignited interest in exploring hydridoborates as SSEs. Similar to LiBH_4 , salts of polyhedral boranes in their HT phase typically exhibit elevated ionic conductivities, attributed to the enhanced rotational motion of the anions. In the HT phase, the crystal structure becomes highly symmetrical, creating a network of interstitial sites within the anionic framework to facilitate cation migration.^[6b,19] Currently, multiple metalhydridoborates with high ionic conductivities have shown potential for application in ASSBs. This family of hydridoborates primarily includes compounds with cations such as Li, Na, K, Mg, Ca, and Ag.^[20] The structures and electrochemical properties of these materials vary significantly depending on the specific cation. For example, NaBH_4 has a lower phase transition temperature than LiBH_4 , and its ionic conductivity remains poor even at elevated temperatures.^[21] $\text{Li}_2\text{B}_{10}\text{H}_{10}$ exhibits a remarkably high phase transition temperature compared to $\text{Na}_2\text{B}_{10}\text{H}_{10}$, for reasons that are not yet understood.^[22] Therefore, there are few reports on

[a] Dr. Z. Lu, Prof. X. Chen
College of Chemistry, Zhengzhou University, Zhengzhou, Henan 450001, China

E-mail: xuenian_chen@zzu.edu.cn

[b] Dr. J.-X. Kang, Dr. P. Qiu, Prof. X. Chen
Henan Key Laboratory of Boron Chemistry and Advanced Materials, School of Chemistry and Chemical Engineering, Henan Normal University, Xinxiang, Henan 453007, China
E-mail: qiuipengtao@htu.edu.cn

these two compounds as SSEs but largely reports on LiBH₄ and Na₂B₁₀H₁₀.

While several excellent reviews have recently addressed hydridoborate SSEs, a systematic and detailed discussion of hydridoborate-based Na-ion electrolytes and their application in Na-metal batteries has not yet been conducted.^[6c,19–20,23] It is both fundamentally important and significant to investigate the status of SSEs based on Na-ion hydridoborates and their applications. In this review, we explore the mechanisms of ionic conduction in pristine hydridoborates, strategies for enhancing ionic conductivity, and their application in ASSMBs. Additionally, we outline future research directions for hydridoborate SSEs to promote their practical application in ASSMBs.

2. Na-Ion Conductivity of Hydridoborates

Orimo et al.^[18] have demonstrated that LiBH₄ exhibits lower conductivities in its low-temperature (LT) phase but achieves superionic conductivity (ionic conductivity in the order of 10^{-3} S cm⁻¹)^[1e] upon transitioning to an HT phase at approximately 117°C. Since then, numerous hydridoborate-based SSEs with fast ionic conductivities have been explored in which most single-anion hydridoborates are at elevated temperatures, where an order-disorder phase transition occurs. As a result, various

approaches have been developed to enhance the RT ionic conductivities of single-anion hydridoborates.

2.1. Ionic Conduction Mechanisms in Single Anion Hydridoborates

NaBH₄ was one of the earliest compounds studied for Na⁺ conduction in hydridoborates. It just showed the ionic conductivity of 2×10^{-10} S cm⁻¹ at 27°C at HT phase of cubic structure.^[21] However, unlike the superionic conductivity observed in LiBH₄, the ionic conductivity of NaBH₄ does not significantly increase with rising temperature, reaching only 10^{-8} S cm⁻¹ at 110°C. In NaBH₄, the tetrahedral BH₄⁻ groups exhibit significant distortion, oriented in two vertical directions, with B–H bond lengths ranging from 1.118 to 1.151 Å and H–B–H bond angles between 98.7° and 113°.^[24] Sodium octahydridotriborate (NaB₃H₈) demonstrates an ionic conductivity of 1.3×10^{-6} S cm⁻¹ at RT and a liquid-like ionic conductivity of 0.05 S cm⁻¹ at 56°C after undergoing an order-disorder phase transformation at approximately 52°C, showcasing excellent conductivity performances.^[11b] The activation energy decreases from 1.66 eV in the LT phase to 0.35 eV in the HT phase, a characteristic typical of superionic materials. Within this B₃H₈⁻ anion, the three boron atoms form an isosceles triangle, characterized by B–B–B bond angles of 59.79° and 60.42° and



Zhiwei Lu received his BS degree from Xinlian College of Henan Normal University and MS degree from Henan Normal University. Now he is pursuing his PhD degree in College of Chemistry, Zhengzhou University. His research focuses on the synthetic and application hydridoborates as the solid-state electrolyte materials in sodium/potassium metal batteries.



Xuenian Chen received his BS and MS degrees from Lanzhou University in China, and his PhD from Lanzhou Institute of Chemical Physics, Chinese Academy of Sciences. He did post-doctoral work and was then appointed Research Scientist at the Department of Chemistry and Biochemistry and the Department of Materials Science and Engineering at The Ohio State University. He is currently a professor in College of Chemistry, Zhengzhou University, China. His research interests are in boron chemistry, organometallics, catalysis, and materials science.



Jia-Xin Kang received his BS degree from the School of Chemical and Environment Science, Shanxi University of Technology. Now he is pursuing his PhD degree in School of Chemistry and Chemical Engineering, Henan Normal University. His research focuses on the application of carbon-based two-dimensional materials in catalysis and the reaction mechanism of boron-containing molecules.



Pengtao Qiu received his BS degree from Henan University of Science and Technology, and his PhD from Xi'an Jiaotong University. He joined the School of Chemistry and Chemical Engineering, Henan Normal University in 2017. His research interests mainly focus on hydridoborate-based solid-state electrolyte materials and sodium/potassium metal batteries.

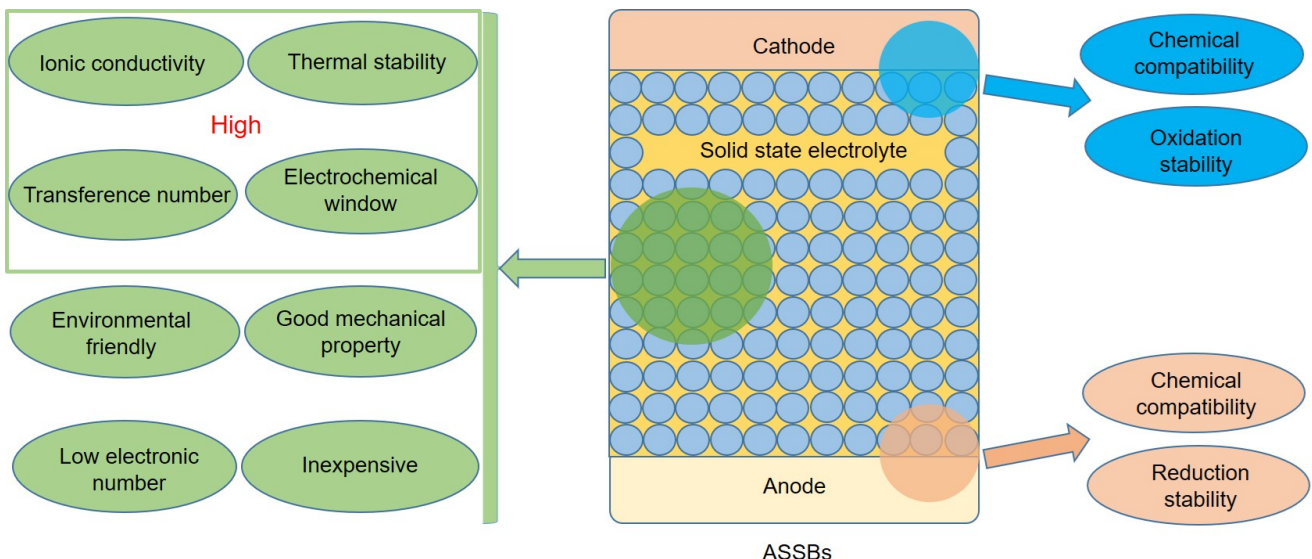


Figure 1. The schematic composition of ASSBs and certain requirements issues for SSE application in ASSBs.

B–B bond lengths of 1.78 Å and 1.77 Å. The anion also includes two B–H–B bridges with B–H bond lengths of 1.16 Å and 1.42 Å and three BH₂ groups, where the B–H bond lengths range from 0.99 to 1.12 Å. The sodium atom is positioned within the mirror plane of the anion, coordinating with four anions in a distorted trigonal prismatic geometry, and Na–H distances spanning from 2.35 to 2.71 Å.^[11b]

Except NaBH₄ and NaB₃H₈, polyhedral boranes of *closo*-hydridoborates and *nido*-hydridoborates have also garnered significant attention from researchers in SSEs due to their high thermal and chemical stability,^[25] and the relative structural diagrams and distinct Mulliken charges of H atoms associated with the numbers structurally are shown in Figure 2. For *arachno*-boranes, the structure (B_nH_{n+6}) are derived from *closo*-

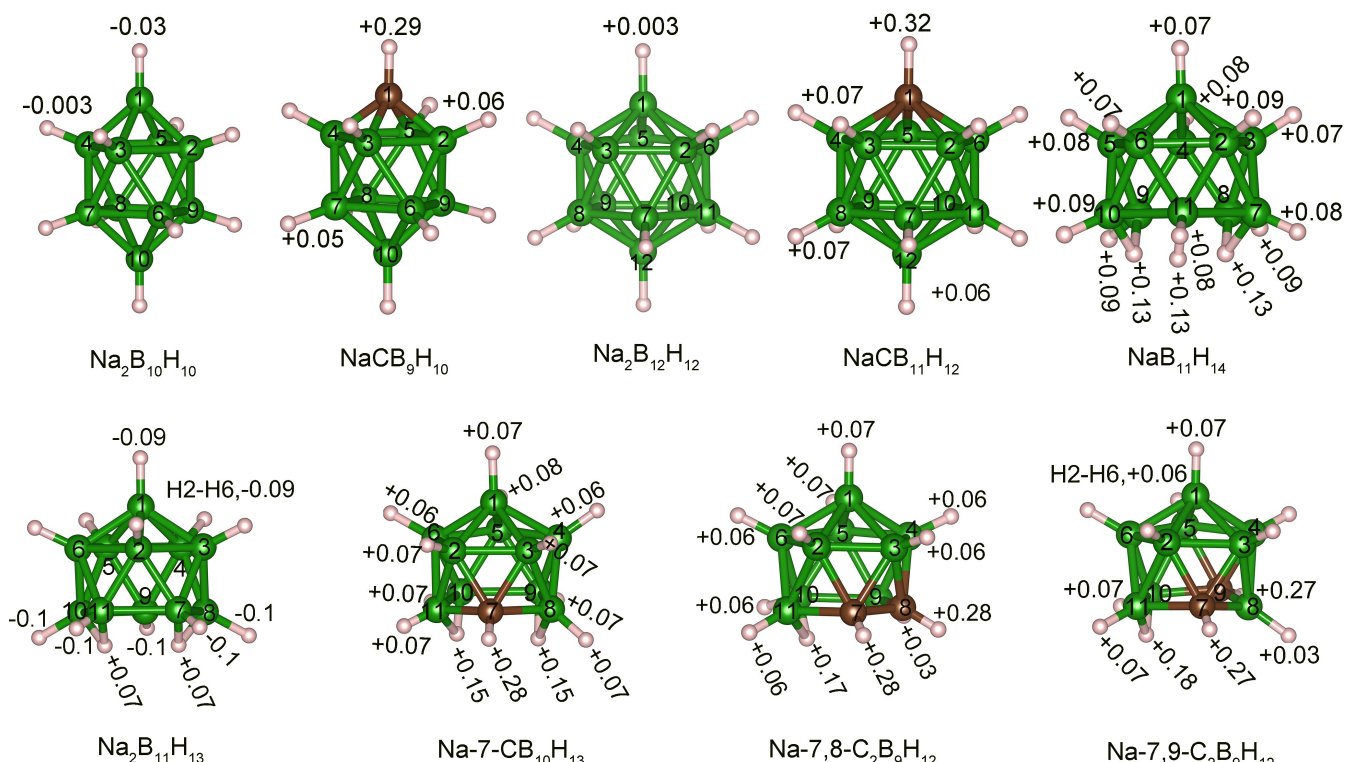


Figure 2. Relative structural diagrams of *closo*-type anions and *nido*-type anions of hydridoborates. The green, brown, and white spheres denoting boron, carbon, and hydrogen atoms, respectively. Distinct Mulliken charges of H atoms associated with the numbers structurally of Na₂B₁₀H₁₀, NaCB₉H₁₀,^[28a] Na₂B₁₂H₁₂, NaCB₁₁H₁₂,^[28b] NaB₁₁H₁₄, Na-7-CB₁₀H₁₃, Na-7,8-C₂B₉H₁₂, and Na-7,9-C₂B₉H₁₂.^[29] Mulliken charges in Na₂B₁₁H₁₃ was determined by first-principles calculations.

borane deltahedra (series of anions formula $[B_nH_n]^{2-}$ for $n=5$ to 12) by removing two BH units, e.g., B occupies n vertices of an $n+2$ deltahedron. Due to their thermal instability at RT, there are no reports on the application of *arachno*-boranes in SSEs.

In *closo*-hydridoborates, sodium decahydro-*closo*-decaborate ($Na_2B_{10}H_{10}$, with a $B_{10}H_{10}^{2-}$ skeleton featuring a double-capped tetragonal antiprism structure) exhibits a disordered face-centered cubic (fcc) structure above 107°C, characterized by an ellipsoidal anion and a vacancy-rich cation sublattice.^[26] This mobile cation sublattice, within the spacious corridors formed by the $B_{10}H_{10}^{2-}$, achieves a remarkable superionic conductivity of 0.01 S cm⁻¹ at 110°C. $Na_2B_{12}H_{12}$ ($B_{12}H_{12}^{2-}$ forms a regular icosahedral structure) undergoes an order-disorder phase transition (from an LT-ordered monoclinic to an HT-disordered cubic phase) at approximately 256°C, with ionic conductivity exceeding 0.1 S cm⁻¹ above the phase transition temperature.^[27] Superionicity in these materials was due to the high rotational mobility and large size of the quasispherical $B_{10}H_{10}^{2-}$ and $B_{12}H_{12}^{2-}$ anions in the disordered phase.

Due to the high ionic conductivities of $Na_2B_{10}H_{10}$ and $Na_2B_{12}H_{12}$, research extended to monovalent *closo*-carborates, where the apical B–H vertices in $B_{10}H_{10}^{2-}$ and $B_{12}H_{12}^{2-}$ were replaced by isoelectronic C–H group. Similar to $Na_2B_{10}H_{10}$ and $Na_2B_{12}H_{12}$, ionic conductivity jumps were observed in $NaCB_9H_{10}$ and $NaCB_{11}H_{12}$ during their order-disorder transitions, occurring at 40°C and 107°C, respectively.^[28] These materials exhibit superionic conductivities exceeding 0.1 S cm⁻¹ at 100°C for $NaCB_9H_{10}$ and 0.12 S cm⁻¹ at 110°C for $NaCB_{11}H_{12}$. Notably, $NaCB_9H_{10}$ retains a high ionic conductivity of 0.03 S cm⁻¹ at RT after cooling, attributed to the hysteretic behavior of its HT-disordered structure, as confirmed by DSC and NMR results. The activation energy of Na^+ conduction is 0.21 eV for $NaCB_9H_{10}$ and 0.22 eV for $NaCB_{11}H_{12}$.^[28] Their conductivity is comparable to traditional ceramic materials like Na β-alumina SSEs and Na superionic conductors (NASICON), which have gained significant attention for applications in sodium-ion batteries. The comparison of Mulliken charges between $CB_{n-1}H_n^-$ ($n=10, 12$) and $B_nH_n^{2-}$ ($n=10, 12$) in Figure 2 suggests that the apical H atom in the C–H bond has a higher positive charge compared to the other H atoms in B–H bond which would influence the anion orientations in the surrounding cations. The $CB_{n-1}H_n^-$ ($n=10, 12$) anions were more oriented and avoided being close to the neighboring cations, compared to $B_nH_n^{2-}$ ($n=10, 12$). The reduction in phase transition temperature and enhancement of ionic migration in these monovalent systems can be attributed to the weaker interactions between the anions and cations and the dipolar moment, which effectively promotes a fluctuating energy landscape. Hence, $NaCB_{n-1}H_n$ ($n=10, 12$) exhibits lower transition temperatures, higher ionic conductivities, and lower activation energies than $Na_2B_nH_n$ ($n=10, 12$).^[28]

The *nido*-boranes, characterized by their open-cage structures, were similar to the cage-like *closo*-structure but with one vertices completely removed and additional compensating bridging and/or terminal H atoms. These structures have also been widely investigated as potential SSEs. The ionic conductivity of $Na_2B_{11}H_{13}$ is 2.5×10^{-7} S cm⁻¹ at 30°C, which suddenly increases to 2.9×10^{-4} S cm⁻¹ at 100°C during heating.^[30] Unlike $Na_2B_{10}H_{10}$

and $Na_2B_{12}H_{12}$, where a step-function type increase in ionic conductivity is associated with an order–disorder polymorphic transition, the polymorphic phase transition in $Na_2B_{11}H_{13}$ occurs around 170°C upon heating. The abrupt increase in ionic conductivity could be attributed to the presence of tetrahydrofuran (THF) in $Na_2B_{11}H_{13}$. The ionic conductivity of $NaB_{11}H_{14}$ is 4.5×10^{-2} S cm⁻¹ at 140°C, with a phase transition occurring at 88°C.^[29] Although the unit cells of $Na_2B_{11}H_{13}$ and $NaB_{11}H_{14}$ were similar in size, the higher ionic conductivity in $NaB_{11}H_{14}$ may be due to fewer vacant sites for cation hopping, given that $Na_2B_{11}H_{13}$ contains twice the Na^+ for charge balancing. Building on the excellent ionic conductivity exhibited by $CB_{n-1}H_n^-$ ($n=10$ and 12), the monocharged *nido*-undeca(carba)borate anion $7-CB_{10}H_{13}^-$, $7,8-C_2B_9H_{12}^-$, and $7,9-C_2B_9H_{12}^-$, which are geometrically similar to $B_{11}H_{13}^{2-}$ and $B_{11}H_{14}^-$, have also been studied as potential SSEs.^[29,31] Although the three compounds have similarly shaped anions, the disordered structures of Na -7-CB₁₀H₁₃ and Na -7,9-C₂B₉H₁₂ feature anion orientations in a cubic close-packed arrangement, similar to the high-temperature phases of *closo*-poly(carba)borate compounds. However, Na -7,8-C₂B₉H₁₂ is an exception, forming a polymorph with hexagonal-close-packed anions. Like *closo*-poly(carba)borates, all these compounds possess disordered phases characterized by cation-vacancy-rich structures and highly reorientation anions. These disordered phases exhibit superionic conductivities, although somewhat lower than those of $NaCB_{11}H_{12}$. The ionic conductivities measured for Na -7-CB₁₀H₁₃, Na -7,8-C₂B₉H₁₂, and Na -7,9-C₂B₉H₁₂ at 140°C are 1.3×10^{-2} , 2.8×10^{-3} , and 2.3×10^{-3} S cm⁻¹ with corresponding activation energies of 0.42(2), 0.41(3), and 0.49(3) eV, respectively.^[29] The ionic conductivities of hydridoborates-based Na^+ are summarized in Figure 3a. The individual H atom variation of Mulliken charges in *nido*-borates anions in Figure 2 were small that the relationship between ionic conductivities and Mulliken charges cannot be well determined. We summarized the nest-end hemisphere of the *nido*-anions and *closo*-anions in Figures 3 b–g. Compared to the *closo*-anions, the H atoms of the *nido*-anions show the trend of a more highly polarized arrangement of positive charges, with the higher accumulative positive charge situated on the nest end.^[29,31] Figures 2 and 3 illustrate that the increasing trend in ionic conductivity is proportional to the polarization effect. We can conclude that less polarized anions tend to exhibit higher ionic conductivities, as they facilitate more energetically favorable cation conduction pathways. However, the $B_{12}H_{12}^{2-}$ anion, with its low polarization, should theoretically have high ionic conductivity. However, its double negative charge requires more cations for charge compensation, which reduces the number of available cation vacancies and, thus, lower conductivities. This explains why the conductivity of $Na_2B_{12}H_{12}$ was lower than expected compared to other compounds.^[29] The trend of decreasing conductivity in these Na *nido*-compounds as the lattice volume decreases aligns with predictions based on lattice volume effects on cation conductivity. Additionally, differences in conductivity may also be influenced by variations in the polarization of the different anions.

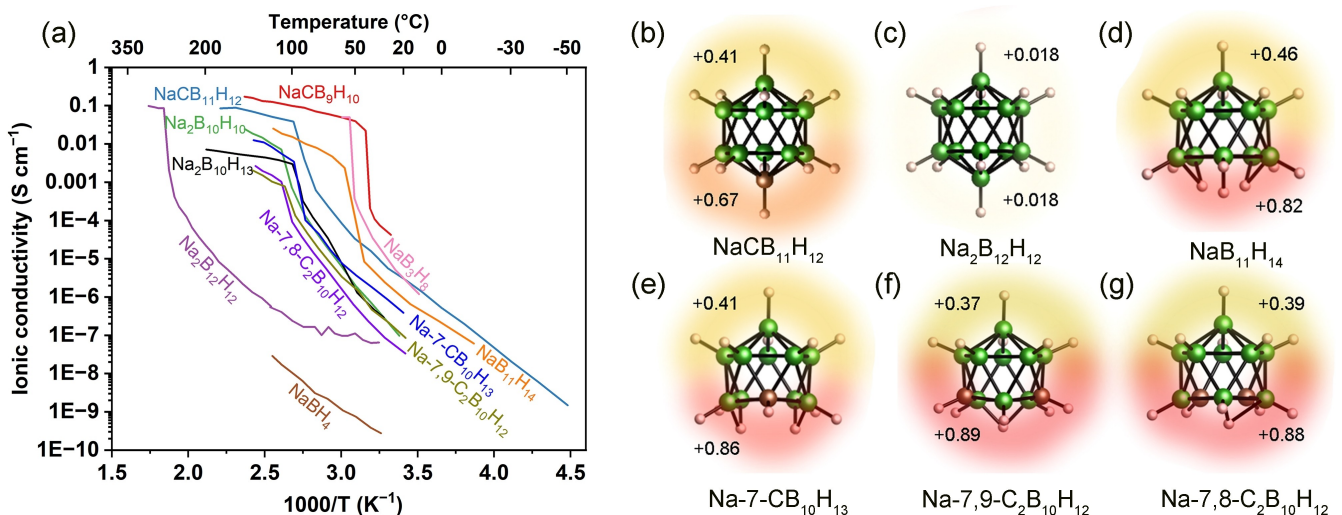


Figure 3. (a) Ionic conductivities of hydridoborates based Na^+ from refs. [8b,11b, 26–31], combined Mulliken charges of groupings H atoms for each hemisphere of the different isolated *nido*-anions, (b) $\text{CB}_{11}\text{H}_{12}^-$ (reprinted with permission from ref. [28b] Copyright 2015 The Royal Society of Chemistry), (c) $\text{B}_{12}\text{H}_{12}^{2-}$ (reprinted with permission from ref. [28b] Copyright 2015 The Royal Society of Chemistry), (d) $\text{B}_{11}\text{H}_{14}^-$ (reprinted with permission from ref. [29] Copyright 2017 American Chemical Society), (e) $7\text{-CB}_{10}\text{H}_{13}^-$ (reprinted with permission from ref. [29] Copyright 2017 American Chemical Society), (f) $7,9\text{-C}_2\text{B}_9\text{H}_{12}^-$ (reprinted with permission from ref. [29] Copyright 2017 American Chemical Society) and (g) $7,8\text{-C}_2\text{B}_{10}\text{H}_{12}^-$ (reprinted with permission from ref. [29] Copyright 2017 American Chemical Society).

2.2. Strategies for Improving Ionic Conductivities

While most hydridoborates exhibit superionic conductivities at HT, their inadequate ionic conductivities at RT fall short of the requirements for practical application in ASSMBs. Consequently, significant efforts have been devoted to enhancing ionic conductivities at LT.

Anion mixing and substitution were effective strategies for enhance ionic conductivity by creating distinct crystal structures or lowering the phase transition temperature in LT. Mixing hydridoborates with similarly sized anions can stabilize HT phase precursor materials. For instance, the HT phase of $\text{NaCB}_9\text{H}_{10}$ can be stabilized in $\text{Na}_2\text{CB}_{11}\text{H}_{12}\text{CB}_9\text{H}_{10}$ (Figure 4a), which exhibits an exceptionally high ionic conductivity of $\sim 7 \times 10^{-2} \text{ S cm}^{-1}$ at 27°C –the highest reported value for hydridoborates to date.^[32] Similarly, $\text{Na}_{3-x}(\text{CB}_{11}\text{H}_{12})_x(\text{B}_{12}\text{H}_{12})_{2x}$ exhibits the HT phase structure of $\text{Na}_2\text{B}_{12}\text{H}_{12}$ with body-centered cubic packing, while $\text{Na}_{11}(\text{B}_{11}\text{H}_{14})_3(\text{B}_{11}\text{H}_{13})_4$ partially stabilizes the HT phase of $\text{Na}_2\text{B}_{11}\text{H}_{13}$ at RT, showing a conductivity of $4.7 \times 10^{-5} \text{ S cm}^{-1}$ at 30°C .^[30,33] Mechanical milling and heat treatment of an equimolar mixture of $\text{Na}_2\text{B}_{10}\text{H}_{10}$ and $\text{Na}_2\text{B}_{12}\text{H}_{12}$ results in a phase-pure compound, $\text{Na}_4\text{B}_{10}\text{H}_{10}\text{B}_{12}\text{H}_{12}$, with a face-centered cubic structure (Figure 4b), identical to the HT phase of $\text{Na}_2\text{B}_{10}\text{H}_{10}$ above 100°C .^[34] Other ratios can partially stabilize the HT phase structure of $\text{Na}_2\text{B}_{12}\text{H}_{12}$, which remains stable at elevated temperatures above 450°C with slightly expanded lattice parameters. $\text{Na}_2\text{BH}_4\text{NH}_2$ exhibits ionic conductivity of $2 \times 10^{-6} \text{ S cm}^{-1}$ at 27°C , four orders of magnitude higher than those of NaBH_4 and NaNH_2 .^[35] The ionic conductivity increases to $7.56 \times 10^{-4} \text{ S cm}^{-1}$ at 90°C , with a low activation energy of 0.67 eV. This improvement is attributed to its specific antiperovskite-type structure with Na^+ site vacancies to facilitate ionic migration.

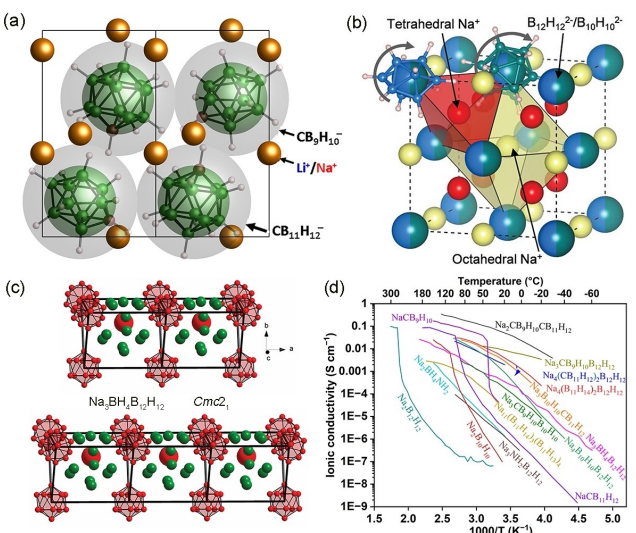


Figure 4. (a) The disordered hexagonal structure of $\text{Na}_2\text{CB}_{11}\text{H}_{12}\text{CB}_9\text{H}_{10}$ (reprinted with permission from ref. [32] Copyright 2016 American Chemical Society), (b) simplified structure of $\text{Na}_2\text{B}_{10}\text{H}_{10}\text{B}_{12}\text{H}_{12}$ based on the HT phase of $\text{Na}_2\text{B}_{10}\text{H}_{10}$ (reprinted with permission from ref. [16a] Copyright 2017 The Royal Society of Chemistry), (c) crystal structure of $\text{Na}_3\text{BH}_4\text{B}_{12}\text{H}_{12}$ (reprinted with permission from ref. [16b] Copyright 2015 WILEY-VCH Verlag GmbH & Co. KGaA, Weinheim), and (d) temperature-dependent conductivities of anion mixing and substitution.

$\text{Na}_3\text{BH}_4\text{B}_{12}\text{H}_{12}$ shows an ionic conductivity of approximately $5 \times 10^{-4} \text{ S cm}^{-1}$ at RT, with an activation energy of 340 meV (Figure 4c), and $\text{Na}_3\text{NH}_2\text{B}_{12}\text{H}_{12}$ exhibits an ionic conductivity of just $1 \times 10^{-4} \text{ S cm}^{-1}$ at 100°C .^[16b,36] Both $\text{Na}_3\text{BH}_4\text{B}_{12}\text{H}_{12}$ and $\text{Na}_3\text{NH}_2\text{B}_{12}\text{H}_{12}$ have structures with open framework channels that were favorable to Na^+ diffusion, and the high ionic conductivity observed in these materials were not entropically activated, as they had not undergone an HT phase transition. The Na

conduction channel in $\text{Na}_3\text{NH}_2\text{B}_{12}\text{H}_{12}$ is 1D along the crystallographic c-axis. In Figure 4c, cation positions in $\text{Na}_3\text{BH}_4\text{B}_{12}\text{H}_{12}$ were not definitively determined but were predicted to occupy tetrahedral sites formed by the anions. These tetrahedral sites were only partially occupied, leading to low-dimensional superionicity. The ionic conductivity of anion mixing and substitution are shown in Figure 4d.

Chemical modifications of anions, such as atomic substitutions, can effectively alter both ionic conductivity and phase transition temperatures. The ionic conductivities of $\text{Na}_2\text{B}_{12}\text{H}_{12-x}\text{I}_x$ (where hydrogen atoms are partially substituted by iodine) reach nearly $10^{-1} \text{ S cm}^{-1}$ at 87°C , with a low activation energy of 140 meV.^[37] This superionic conductivity is comparable to that of $\text{NaCB}_{11}\text{H}_{12}$ that may be attributed to the minor modification of the anion, leading to a new hexagonal close-packed (hcp) structure in $\text{Na}_2\text{B}_{12}\text{H}_{12-x}\text{I}_x$ rather than the body-centered cubic (bcc) structure observed in the HT phase of $\text{Na}_2\text{B}_{12}\text{H}_{12}$. The hcp anionic backbone offers a more favorable framework for ionic conduction among close-packed lattices, facilitating O–O (octahedral), T–T (tetrahedral), and T–O–T cation hops. However, all halide substitution could lead to an increased structural transition temperature and decreased ionic conductivity. The structures of $\text{Na}_2\text{B}_{12}\text{X}_{12}$ ($\text{X}=\text{Cl}, \text{Br}, \text{I}$) were all isostructural at RT, transitioning into Fm3m at HT.^[38] The high transition temperature and low ionic conductivity of $\text{Na}_2\text{B}_{12}\text{X}_{12}$ are likely due to the larger size and mass of the anions and the increased strength and directionality of Na–X interactions, which restrict cation dynamic motion (Figure 5a). A series of iodinated *closو-decarobates*, $\text{Na}_2\text{B}_{10}\text{H}_{10-n}\text{I}_n$ ($n=1, 2$, and 10), exhibit an amorphous structure.^[39] The ionic conductivity increases with higher iodine

content, but all remains lower than $\text{Na}_2\text{B}_{10}\text{H}_{10}$. A similar trend was observed in halogenated monocarba-*closو-decarobates*, such as $\text{NaCHB}_9\text{H}_8\text{-Br}$, $\text{NaCHB}_9\text{H}_8\text{-I}$, and $\text{NaCHB}_9\text{H}_4\text{-6,7,8,9,10-I}_5$, in which both ionic conductivity and thermal stability are lower than those of $\text{NaCB}_9\text{H}_{10}$.^[40] $\text{NaHCB}_{11}\text{H}_5\text{Cl}_6$ and $\text{NaHCB}_{11}\text{H}_5\text{Br}_6$ compounds exhibit order–disorder transitions at 203 and 218°C , respectively, and display Na superionic conductivity in the HT phase.^[41] The ionic conductivities were lower than $\text{NaCB}_{11}\text{H}_{12}$, but the decomposition temperatures were over 400°C , making them potential in HT battery applications. These ionic conductivities decreased when halide substitution can be explained by the increased volume, mass, and electrostatic potential of the iodinated anions, which hinder ionic mobility. Theoretical calculations of the electrostatic potential (ESP) for $\text{Na}_2\text{B}_{10}\text{H}_{10-n}\text{I}_n$ ($n=1, 2$, and 10) (Figure 5b), $\text{NaCHB}_9\text{H}_8\text{-6-Br}$, $\text{NaCHB}_9\text{H}_8\text{-6-I}$, and $\text{NaCHB}_9\text{H}_4\text{-6,7,8,9,10-I}_5$ (Figure 5c) suggest a close connection between anisotropic electron densities in cations and anions that increased the diffusion barriers that decreased their ionic conductivities. The ionic conductivity of chemical modifications of anions is shown in Figure 5d.

Oxidation of hydridoborates is another novel approach to tuning the ionic conductivity. When NaBH_4 is exposed to 5% O_2 , surface atoms rearrange, resulting in the compound with an ionic conductivity of approximately $10^{-3} \text{ S cm}^{-1}$ at 35°C .^[42] Compared to NaBH_4 , the observed lower Bragg angles of oxidized NaBH_4 without significant changes in structure suggest a defective crystalline structure. The absence of oxide phases indicates that oxidation occurs only on the NaBH_4 surface, which may be amorphous or lack long-range crystallinity. *Closو-borates* have demonstrated great potential as ideal SSEs, and the oxidation of $\text{B}_{10}\text{H}_{10}^{2-}$ and $\text{B}_{12}\text{H}_{12}^{2-}$ to formed *conjuncto-hydridoborate* $\text{B}_{20}\text{H}_{18}^{2-}$, $\text{B}_{20}\text{H}_{18}^{4-}$, $\text{B}_{24}\text{H}_{23}^{3-}$, and $\text{B}_{36}\text{H}_{34}^{4-}$ had shown promise as effective strategies for improving both ionic conductivities and electrochemical stability.^[43] $\text{Na}_2\text{B}_{20}\text{H}_{18}$ and $\text{Na}_4\text{B}_{20}\text{H}_{18}$ (${}^1\text{B}$ NMR spectra and structures in Figure 6a) exhibited higher ionic conductivity of $2.5 \times 10^{-6} \text{ S cm}^{-1}$ and $3.8 \times 10^{-6} \text{ S cm}^{-1}$, respectively, than $\text{Na}_2\text{B}_{10}\text{H}_{10}$ ($1.7 \times 10^{-7} \text{ S cm}^{-1}$ at RT).^[43a,b] Similar trends are observed in $\text{Na}_3\text{B}_{24}\text{H}_{13}$ and $\text{Na}_4\text{B}_{36}\text{H}_{34}$, which are derived from $\text{Na}_2\text{B}_{12}\text{H}_{12}$.^[43c,d] The structures of $\text{Na}_3\text{B}_{24}\text{H}_{13}$ (${}^1\text{B}$ NMR spectra and structures in Figure 6b) and $\text{Na}_4\text{B}_{36}\text{H}_{34}$ (${}^1\text{B}$ NMR spectra and structures in Figure 6c) were amorphous, with RT ionic conductivities of $2.3 \times 10^{-5} \text{ S cm}^{-1}$ and $1.71 \times 10^{-5} \text{ S cm}^{-1}$, nearly two orders of magnitude higher than $\text{Na}_2\text{B}_{12}\text{H}_{12}$ ($2.7 \times 10^{-7} \text{ S cm}^{-1}$). Notably, these *conjuncto-hydridoborates* had lower activation energies and did not exhibit phase transitions compared to raw materials. The increased ionic conductivity in *conjuncto-hydridoborates* can be attributed to their larger anion sizes, which provide more vacant sites conducive to the formation of an efficient Na diffusion network. Moreover, mixing *conjuncto-hydridoborate* and $\text{Na}_2\text{B}_{12}\text{H}_{12}$ results in enhanced ionic conductivity compared to the starting materials, showing great potential as SSEs. $\text{Na}_2\text{B}_{20}\text{H}_{18} \cdot 4\text{Na}_2\text{B}_{12}\text{H}_{12}$ and $\text{Na}_4\text{B}_{20}\text{H}_{18} \cdot 3\text{Na}_2\text{B}_{12}\text{H}_{12}$ exhibit fast ionic conductivities exceeding $2.8 \times 10^{-4} \text{ S cm}^{-1}$ and $2.2 \times 10^{-4} \text{ S cm}^{-1}$ at RT, respectively. The composites $\text{Na}_3\text{B}_{24}\text{H}_{23} \cdot 5\text{Na}_2\text{B}_{12}\text{H}_{12}$ and $\text{Na}_4\text{B}_{36}\text{H}_{24} \cdot 7\text{Na}_2\text{B}_{12}\text{H}_{12}$ demonstrate high ionic conductivities of $1.4 \times 10^{-3} \text{ S cm}^{-1}$ and $1.02 \times 10^{-3} \text{ S cm}^{-1}$ at RT. The ionic conductivity of *conjuncto-hydridoborate* anions is shown in Figure 6d.

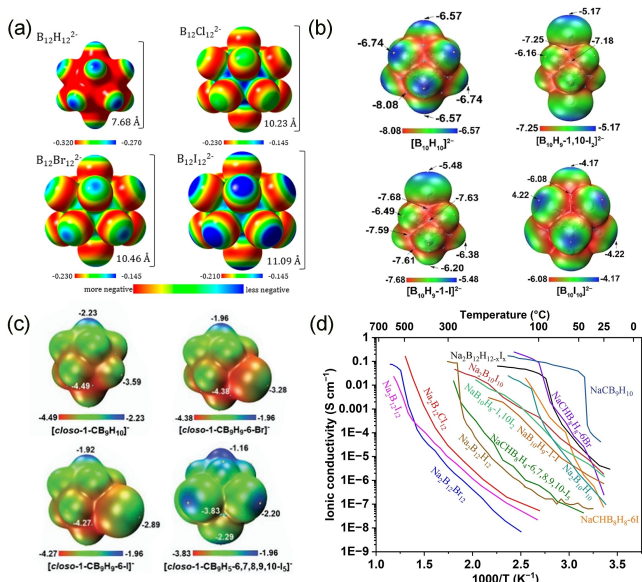


Figure 5. (a) $\text{B}_{12}\text{X}_{12}^{2-}$ ($\text{X}=\text{Cl}, \text{Br}, \text{I}$) (reprinted with permission from ref. [38]. Copyright 2017 American Chemical Society), (b) the ESP of $\text{Na}_2[\text{B}_{10}\text{H}_{10-n}\text{I}_n]$ ($n=1, 2, 10$) (reprinted with permission from ref. [39]. Copyright 2021 American Chemical Society), (c) The ESP of $\text{Na}[1\text{-CHB}_9\text{H}_{g-n}\text{X}_n]$ ($n=1, 5$ and $\text{X}=\text{Br}, \text{I}$) and $\text{Na}[\text{closо-1-CHB}_9\text{H}_g\text{-6-Br}]$ ($n=10$) (reprinted with permission from ref. [40]. Copyright 2021 The Royal Society of Chemistry and the Chinese Chemical Society), and (d) Temperature-dependent conductivities of atomic substitution anion.

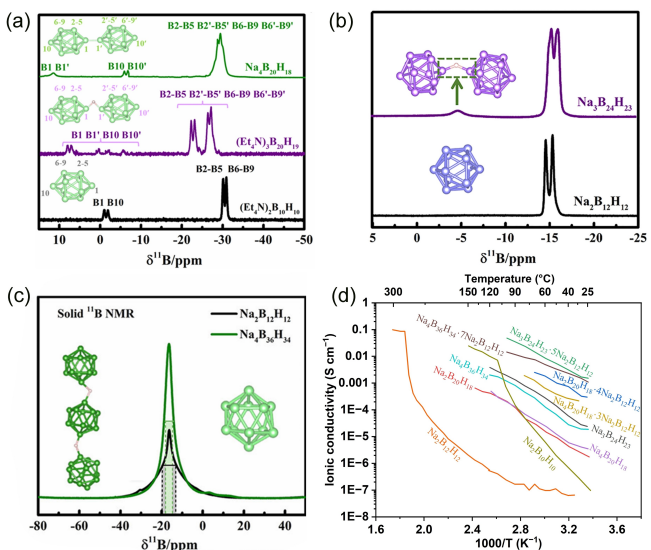


Figure 6. (a) ^{11}B NMR spectra and structures of $\text{Na}_4\text{B}_{20}\text{H}_{18}$ (reprinted with permission from ref. [43b] Copyright 2022 American Chemical Society), (b) ^{11}B NMR spectra and structures of $\text{Na}_3\text{B}_{24}\text{H}_{23}$ (reprinted with permission from ref. [43c] Copyright 2022 Elsevier B.V.), (c) ^{11}B NMR spectra and structures of $\text{Na}_4\text{B}_{36}\text{H}_{34}$ (reprinted with permission from ref. [43d] Copyright 2022 American Chemical Society), and (d) Temperature-dependent ionic conductivities of conjuncto-hydridoborate and conjuncto-hydridoborate/ $\text{Na}_2\text{B}_{12}\text{H}_{12}$.

Morphological modification through ball milling can partially stabilize the HT phases of large-anion *closو*-borates at LT, as the schematic diagram shows in Figure 7a. It can be seen that the presence of these superionic structures significantly enhances their conductivity. According to the Scherrer equation, the particle size of orthorhombic-structured crystallites in $\text{NaCB}_{11}\text{H}_{12}$ decreases from 44 nm to 26 nm, and the particle size of monoclinic-structured crystallites in $\text{Na}_2\text{B}_{10}\text{H}_{10}$ decreases from 32 nm to 23 nm after ball milling.^[44] Similar results are observed in $\text{Na}_2\text{B}_{12}\text{H}_{12}$. The stabilization of the HT phase at LT is attributed to the reduction in crystallite size and introduces nano defects such as interstitial sites, dislocations, vacancies, grain boundaries, and stacking faults that could provide more vacant sites that facilitate ionic diffusion. For ball-milled NaB_3H_8 , the XRD patterns do not show the presence of superionic structures even though the ionic conductivity is nearly an order of magnitude higher than that of unprocessed NaB_3H_8 in the first cycle.^[11b] This increase in ionic conductivity is likely due to the defects formed

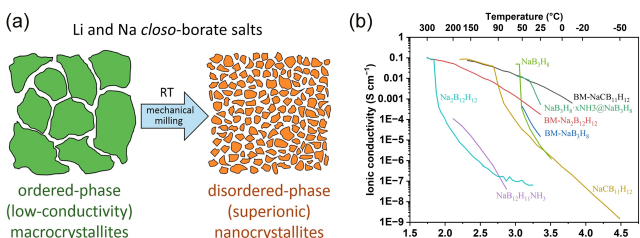


Figure 7. (a) schematic diagram of mechanical milling (reprinted with permission from ref. [44] Copyright 2016 Elsevier B.V.) and (b) Temperature-dependent conductivities of mechanical milling, amination of $\text{B}_{12}\text{H}_{12}^{2-}$ and NaB_3H_8 .

during ball milling. However, the continued decrease in ionic conductivity with repeated heating/cooling cycles may be due to the reduction of these defects, which anneal out at HT. The corresponding ionic conductivity is shown in Figure 7b.

In addition to the previously discussed methods for enhancing ionic conductivity, the effects of the NH_3 group in hydridoborates have been examined. Unlike the less negatively charged $\text{B}_{12}\text{X}_{12}^{2-}$ ($\text{X}=\text{H}, \text{Cl}, \text{Br}, \text{I}$) and similar to $\text{CB}_{11}\text{H}_{12}^-$, the amination of $\text{B}_{12}\text{H}_{12}^{2-}$ with hydroxylamine–O–sulfonic acid to synthesize $\text{NaB}_{12}\text{H}_{11}\text{NH}_3$ results in a monovalent, weakly coordinating anion, indicating a lower cation concentration.^[45] The α - $\text{NaB}_{12}\text{H}_{11}\text{NH}_3$ structure did not have longer Na–Na jump distances compared to $\text{Na}_2\text{B}_{12}\text{H}_{12}$, and its ionic conductivity is $4.2 \times 10^{-8} \text{ S cm}^{-1}$ at 75 °C and $1.2 \times 10^{-4} \text{ S cm}^{-1}$ at 200 °C. This lower ionic conductivity relative to $\text{Na}_2\text{B}_{12}\text{H}_{12}$ may be attributed to the reduced Na concentration in α - $\text{NaB}_{12}\text{H}_{11}\text{NH}_3$. Additionally, incorporating NH_3 into NaB_3H_8 to form $\text{NaB}_3\text{H}_8 \cdot x\text{NH}_3 @ \text{NaB}_3\text{H}_8$ exhibits a higher ionic conductivity than NaB_3H_8 , with a value of $8.4 \times 10^{-4} \text{ S cm}^{-1}$ at RT and reaching $2.1 \times 10^{-2} \text{ S cm}^{-1}$ at 45 °C, making it suitable for battery applications.^[11a] The ionic conductivity decreased from 1.87 to $1.13 \times 10^{-3} \text{ S cm}^{-1}$ after being stored at 30 °C for one month, possibly due to slow aging.

Most hydridoborates exhibit superionic conductivities at HT, showing great potential for application as SSEs. Singly charged polyanion salts tend to have higher conductivities than their analogs at similar temperatures. Various strategies have been developed to improve the poor ionic conductivities at RT, including stabilizing superionic phases at LT and altering the anisotropic electron densities in cations and anions to enhance cation mobility. So far, many boranes have demonstrated promising potential for practical application in ASSMBs.

3. Application of Hydridoborates in ASSMBs

ASSMBs have the potential to meet the growing demand for high-performance energy storage. Among their components, SSEs play a critical role in determining the overall performance of ASSMBs. The ideal SSEs must have high thermal stability, good deformability, and high electrochemical stability against oxidation and reduction. High thermal stability and good deformability ensure easy processing and operation in a wide temperature range. High electrochemical stability could make the ASSMBs with the high power density. Additionally, the SSEs should be mechanically robust to maintain tight contact with electrode materials. Hydridoborate-based Na-ion SSEs, with their high ionic conductivity, chemical stability, electrochemical stability, and ability to prevent dendrite formation, show great promise in enhancing the performance of ASSMBs, in particular, when used with metallic anodes during charge and discharge cycles.

3.1. Thermal and Electrochemical Stability Window (ESW) of Hydridoborate-Based Na-Ion SSEs

The high thermal stability of SSEs is particularly attractive because they could provide higher safety in ASSMBs. The

thermal decomposition temperature of *closo*-borates ($\text{Na}_2\text{B}_{10}\text{H}_{10}$ and $\text{Na}_2\text{B}_{12}\text{H}_{12}$) occurs above 350°C ^[46] and *closo*-carbaborates ($\text{NaCB}_9\text{H}_{10}$ and $\text{NaCB}_{11}\text{H}_{12}$) are thermally stable above 200°C based on the DSC measurement.^[32,47] The high thermal stability of *closo*-(carba)borates could be explained by a 3D aromaticity closed-cage structure with high chemical stability and higher bond energy between B–B and B–C bonds.^[48] The thermal decomposition temperature of *nido*-borates with open-cage structures is at a lower temperature range of 100°C to 200°C .^[29] It could be attributed to the loss of quasispherical geometry, making the electron delocalization reduction and resulting in lower electrochemical/chemical stability in the *nido*-frameworks compared to *closo*-frameworks. For NaB_3H_8 , it exhibits the lowest thermal stability and decomposes at 65°C .^[11b]

The electrochemical stability of SSEs estimated based on LSV measurements can determine the energy density of ASSMBs. Several Li- and Na- hydridoborate-based SSEs that were claimed

with outstandingly wide ESW have been tested in fast operating sweeping rates, then these SSEs were revised with more appropriate setups, leading to the determination of narrower, more realistic voltage windows. For example, previously experimental tested ESW for LiBH_4 was 5 V, but calculations and battery applications were about $\sim 2\text{ V}$ in later reported.^[20,49] This also could be found in $\text{Na}_2\text{B}_{10}\text{H}_{10}$ and $\text{NaCB}_9\text{H}_{10}$, as shown in Table 1. The ESW were above 4.0 and 5.0 V in $\text{Na}_2\text{B}_{10}\text{H}_{10}$ and $\text{NaCB}_9\text{H}_{10}$ at sweeping rates of 5 mVs^{-1} , but dropped to 3.0 and 3.75 V at the sweeping rates of 0.1 mVs^{-1} and 0.02 mVs^{-1} . This difference was due to the high sweeping rates of above $> 1\text{ mV}$ that lack diffusivity toward the working electrode, but the oxidation reaction was slow kinetics of the decomposition products. When the LSV was conducted at lower than sweeping rates of 0.1 mVs^{-1} , it had slow reaction kinetics behavior and yielded very large overpotentials and small currents, which were sensitive in the nA range. The obtained ESW in low sweeping

Table 1. ESW and critical current density (CCD) of hydridoborate-based Na-ion SSEs.

Electrolytes	I/E ^[a]	CCD (electrode)/T ^[b]	ESW (V) or O.L. ^[c]	W.E. ^[d]	S.R. ^[e]	Ref.
NaB_3H_8	$0.95/10^{-10}$	0.8 (Na)/30	0.92–3.32	SUS ^[f]	0.1	[11b]
$\text{NaB}_3\text{H}_8\text{-xNH}_3@\text{NaB}_3\text{H}_8$	$0.96/10^{-8}$	2.5 (Na)/30	1.34–3.85	SUS	0.1	[11a]
$\text{Na}_2\text{B}_{10}\text{H}_{10}$	N.R. ^[g]	N.R.	0.5–3.0	SUS	0.1	[43a]
/	/	N.R.	0.5–3.0	C	0.01	[43a]
/	N.R.	N.R.	0–4.0	SUS	5	[26]
$\text{Na}_2\text{B}_{20}\text{H}_{18}$	0.87/ N.R.	N.R.	0.5–8	SUS	0.1	[43a]
/	/	N.R.	0.5–5.1	C	0.01	[43a]
$\text{Na}_2\text{B}_{20}\text{H}_{18}\cdot 4\text{Na}_2\text{B}_{12}\text{H}_{12}$	0.98/N.R.	0.8 (Na)/RT	4.8	C	0.01	[43a]
$\text{Na}_4\text{B}_{20}\text{H}_{18}$	N.R.	N.R.	3.3	C	0.01	[43b]
$\text{Na}_4\text{B}_{20}\text{H}_{18}\cdot 3\text{Na}_2\text{B}_{12}\text{H}_{12}$	0.92/N.R.	0.4 (Na)/RT	3.45	C	0.01	[43b]
$\text{Na}_2\text{B}_{12}\text{H}_{12}$	N.R.	0.2 (Na)/60	3.6	C	0.01	[43c]
$\text{Na}_3\text{B}_{24}\text{H}_{23}$	0.92/N.R.	0.4 (Na)/60	6.7	C	0.01	[43c]
$\text{Na}_3\text{B}_{24}\text{H}_{23}\cdot 5\text{Na}_2\text{B}_{12}\text{H}_{12}$	0.97/N.R.	0.7 (Na)/RT, 1.0 (Na) /60	5.8	C	0.01	[43c]
$\text{Na}_4\text{B}_{36}\text{H}_{34}$	$0.92/10^{-11}$	0.4 (Na)/RT	6.9	C	0.01	[43d]
$\text{Na}_4\text{B}_{36}\text{H}_{34}\cdot 7\text{Na}_2\text{B}_{12}\text{H}_{12}$	$0.97/10^{-11}$	0.9 (Na)/RT	5.5	C	0.01	[43d]
$\text{NaCB}_9\text{H}_{10}$	N.R.	N.R.	>5.0	SUS	5	[28a]
/	N.R.	N.R.	3.8	SUS	0.02	[52]
/	0.999/N.R.	0.7 (Na)/30	3.1	SUS	0.01	[53]
$\text{NaCB}_{11}\text{H}_{12}$	N.R.	N.R.	4.2	SUS	0.02	[52]
/	N.R.	N.R.	4.2	C	0.01	[33a]
$\text{NaB}_{11}\text{H}_{14}$	N.R.	N.R.	2.6	C	0.05	[30]
$\text{Na}_2\text{B}_{11}\text{H}_{13}$	N.R.	N.R.	2.1	C	0.05	[30]
$\text{Na}_{11}(\text{B}_{11}\text{H}_{14})_3(\text{B}_{11}\text{H}_{13})_4$	N.R.	N.R.	2.1	C	0.05	[30]
$\text{Na}_3\text{BH}_4\text{B}_{12}\text{H}_{12}$	N.R.	N.R.	0–10	SUS	50	[16b]
$\text{Na}_3\text{NH}_2\text{B}_{12}\text{H}_{12}$	N.R.	N.R.	0–10	SUS	10	[36]
$\text{Na}_8(\text{B}_{10}\text{H}_{10})(\text{B}_{12}\text{H}_{12})_3$	N.R.	N.R.	0–5	SUS	2	[54]
$\text{Na}_4(\text{B}_{12}\text{H}_{12})(\text{B}_{10}\text{H}_{10})$	N.R.	N.R.	0–3	SUS	3	[16a]
$\text{Na}_4(\text{CB}_{11}\text{H}_{12})_2(\text{B}_{12}\text{H}_{12})$	N.R.	N.R.	4.2	C	0.01	[33a]
/	N.R.	0.6 (Na)/RT	N.R.	N.R.	N.R.	[55]
$\text{Na}_2(\text{BH}_4)(\text{NH}_2)$	$\text{N.R./}10^{-9}$	0.9 (NaSn)/90	0–2	C	0.1	[56]

[a] Ion transference number/Electronic conductivity. [b] Temperature ($^\circ\text{C}$). [c] Oxidative limit. [d] Working electrode [e] Sweeping rates (mV s^{-1}). [f] Stainless steel. [g] Not reported.

rates were highly consistent with calculated oxidation potential and practical application into ASSBs. Furthermore, the results of LSV testing with the SSE-carbon composite show a decreased ESW when compared to the SSE composite for $\text{Na}_2\text{B}_{20}\text{H}_{18}$. However, these findings are consistent with those observed for $\text{Na}_2\text{B}_{10}\text{H}_{10}$ and $\text{NaCB}_{11}\text{H}_{12}$. Hence, the accurate method to evaluate the ESW of hydridoborates was the sweeping rates lower than 0.1 mVs^{-1} and tested with SSE-carbon composite.

As can be seen from Table 1, the anions are sorted from lowest to highest as a function of oxidation voltage: $\text{Na}_2\text{B}_{11}\text{H}_{13}$, $\text{NaB}_{11}\text{H}_{14}$, NaB_3H_8 , $\text{Na}_2\text{B}_{10}\text{H}_{10}$, $\text{Na}_2\text{B}_{12}\text{H}_{12}$, $\text{NaCB}_9\text{H}_{10}$, and $\text{NaCB}_{11}\text{H}_{12}$. The lowest electrochemical stability of *nido*-borates ($\text{Na}_2\text{B}_{11}\text{H}_{13}$ and $\text{NaB}_{11}\text{H}_{14}$) may be attributed to the loss of quasispherical geometry, which makes the electron delocalization reduction. ESW of $\text{Na}_2\text{B}_{10}\text{H}_{10}$ and $\text{Na}_2\text{B}_{12}\text{H}_{12}$ are increasing with aromaticity increasing. This result aligns well with previous reports on the exceptional “aromatic-like” stability of $\text{B}_n\text{H}_n^{2-}$ *closو*-borates, attributed to the enhanced delocalization of the B–B σ-bonds within the polyhedral clusters.^[47b,50] C-substituted anions ($\text{NaCB}_9\text{H}_{10}$ and $\text{NaCB}_{11}\text{H}_{12}$) are more robust than their corresponding unsubstituted counterparts. This increased stability may be due to the differing acidity of the C–H hydrogen being more comparable to that of acetylene.^[51] Higher acidity leads to higher stability of the conjugate base, making the corresponding anion less prone to oxidation. The superior stability of 12-vertex polyhedral among these boranes implies that anion stability is basically dependent on the isotropic delocalization of electrons.^[47a] The introduced isoelectronic C–H group in anion makes them more stable. It is surprising that the *conjuncto*-hydridoborates exhibit an outstanding wide ESW than that of single hydridoborates. The ESW of $\text{Na}_4\text{B}_{36}\text{H}_{34}$ was up to 6.9 V, the highest value in hydridoborate-based Na-ion.

3.2. Compatibility Against Na Anode and CCD

The compatibility of hydridoborate SSEs with the Na anode (ideally alkali metal) and their CCD (generally defined as the maximum current density without cell failure) have been studied in a symmetry cell. The corresponding CCD of hydridoborate-based Na^+ SSEs is shown in Table 1. Since the research on CCD in hydridoborate compounds was neglected in the early stage, many studies on borane compounds did not report these data ($\text{Na}_3\text{BH}_4\text{B}_{12}\text{H}_{12}$, $\text{Na}_4(\text{B}_{12}\text{H}_{12})(\text{B}_{10}\text{H}_{10})$, and $\text{Na}_4(\text{CB}_{11}\text{H}_{12})_2(\text{B}_{12}\text{H}_{12})$ etc.).

The GC curves for $\text{Na}/\text{NaB}_3\text{H}_8/\text{Na}$ cell and $\text{Na}/\text{ball-milled NaB}_3\text{H}_8/\text{Na}$ cells (Figure 8a) with a current density of 0.1 mA cm^{-2} are investigated at 30°C .^[11b] After 300 cycles, the polarization voltage in the $\text{Na}/\text{NaB}_3\text{H}_8/\text{Na}$ cell increased slightly from 0.18 to 0.19 V, while no voltage change was observed in the $\text{Na}/\text{ball-milled NaB}_3\text{H}_8/\text{Na}$ cell. Both NaB_3H_8 and ball-milled NaB_3H_8 exhibited excellent compatibility with the Na anode, demonstrating high electrochemical stability during the Na plating/stripping cycles. NMR and XRD analyses of the $\text{Na}/\text{NaB}_3\text{H}_8$ interface after cycling detected only small amounts of NaBH_4 , further confirming the high stability of Na with NaB_3H_8 . Interestingly, the resistance of the SUS/SSEs/SUS interface was significantly higher than that of the Na/SSEs/Na interface. The measured resistance of SUS/SSEs/SUS interface was about $16.5 \text{ k}\Omega$ at 30°C , decreased by nearly an order of magnitude to $1.9 \text{ k}\Omega$ in the Na/Na cell, suggesting that the contact between NaB_3H_8 and Na metal is tight and the increased effective contact area that significantly enhances ionic conductivity in the Na/Na cell. This conclusion further confirms the excellent compatibility of NaB_3H_8 with the Na anode interface. A sudden voltage drop at 0.8 mA cm^{-2} of NaB_3H_8 observed in Figure 8b indicated that the CCD of NaB_3H_8 is 0.8 mA cm^{-2} . For $\text{NaB}_3\text{H}_8\cdot\text{xNH}_3@\text{NaB}_3\text{H}_8$, the GC curve of the Na/Na cell at a constant current density of 0.2 mA cm^{-2} showed stable polarization voltage around 0.04 V for up to 160 hours. Similar to NaB_3H_8 , NMR and XRD spectra confirmed the formation of NaBH_4 between Na and $\text{NaB}_3\text{H}_8\cdot\text{xNH}_3@\text{NaB}_3\text{H}_8$ during cycling. Although the polarization voltage became unstable at higher current densities, it remained relatively stable at 1 mA cm^{-2} after 250 cycles. A sudden voltage drop at 2.5 mA cm^{-2} of $\text{NaB}_3\text{H}_8\cdot\text{xNH}_3@\text{NaB}_3\text{H}_8$ observed in Figure 8c indicated that the CCD of $\text{NaB}_3\text{H}_8\cdot\text{xNH}_3@\text{NaB}_3\text{H}_8$ is 2.5 mA cm^{-2} . This higher CCD, compared to NaB_3H_8 (0.8 mA cm^{-2}), suggests that introducing the neutral molecule not only increased ionic conductivity but also improved compatibility with Na. The CCD value of $\text{NaB}_3\text{H}_8\cdot\text{xNH}_3@\text{NaB}_3\text{H}_8$ was the highest in hydridoborate SSEs, suggesting excellent capability to suppress the Na dendrite formed. The GC curves of $\text{Na}/\text{NaCB}_9\text{H}_{10}/\text{Na}$ were examined at 60°C and 27°C under an applied stack pressure to ensure good interfacial contact between the SSEs and the Na anode to prevent void formation.^[53] Both cells exhibited increased overpotential during cycling, indicating the formation of an interphase or voids. The CCD of $\text{NaCB}_9\text{H}_{10}$ was investigated by the capacity control protocol with 0.2 mA h cm^{-2} at a stack pressure of 2.7 MPa . The cell was precycled at 0.2 mA cm^{-2} for 200 hours, and each cycle rested for at least two minutes. The potential decreases during the measurements when the current density reaches 1 mA cm^{-2} , indicating void formation. Hence, a current density of 0.7 mA cm^{-2} can be ascribed as the CCD value of

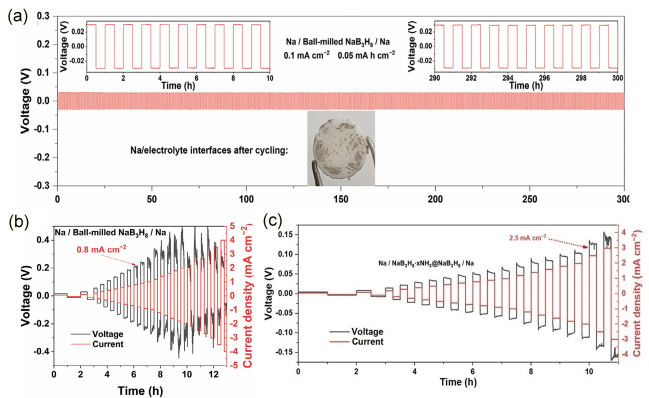


Figure 8. (a) Constant current GC curves of the Na/ball-milled $\text{NaB}_3\text{H}_8/\text{Na}$ cells at a current density of 0.1 mA cm^{-2} with interval of 30 min (reprinted with permission from ref. [11b] Copyright 2024 Wiley-VCH Verlag GmbH & Co. KGaA, Weinheim), (b) Stepped current GC curve of a Na/ball-milled $\text{NaB}_3\text{H}_8/\text{Na}$ cell (reprinted with permission from ref. [11b] Copyright 2024 Wiley-VCH Verlag GmbH & Co. KGaA, Weinheim), (c) Stepped current GC curve of a $\text{Na}/\text{NaB}_3\text{H}_8\cdot\text{xNH}_3@\text{NaB}_3\text{H}_8/\text{Na}$ cell (reprinted with permission from ref. [11a] Copyright 2024 Wiley-VCH Verlag GmbH & Co. KGaA, Weinheim).

ball-milled NaB_3H_8 /SUS was about $16.5 \text{ k}\Omega$ at 30°C , decreased by nearly an order of magnitude to $1.9 \text{ k}\Omega$ in the Na/Na cell, suggesting that the contact between NaB_3H_8 and Na metal is tight and the increased effective contact area that significantly enhances ionic conductivity in the Na/Na cell. This conclusion further confirms the excellent compatibility of NaB_3H_8 with the Na anode interface. A sudden voltage drop at 0.8 mA cm^{-2} of NaB_3H_8 observed in Figure 8b indicated that the CCD of NaB_3H_8 is 0.8 mA cm^{-2} . For $\text{NaB}_3\text{H}_8\cdot\text{xNH}_3@\text{NaB}_3\text{H}_8$, the GC curve of the Na/Na cell at a constant current density of 0.2 mA cm^{-2} showed stable polarization voltage around 0.04 V for up to 160 hours. Similar to NaB_3H_8 , NMR and XRD spectra confirmed the formation of NaBH_4 between Na and $\text{NaB}_3\text{H}_8\cdot\text{xNH}_3@\text{NaB}_3\text{H}_8$ during cycling. Although the polarization voltage became unstable at higher current densities, it remained relatively stable at 1 mA cm^{-2} after 250 cycles. A sudden voltage drop at 2.5 mA cm^{-2} of $\text{NaB}_3\text{H}_8\cdot\text{xNH}_3@\text{NaB}_3\text{H}_8$ observed in Figure 8c indicated that the CCD of $\text{NaB}_3\text{H}_8\cdot\text{xNH}_3@\text{NaB}_3\text{H}_8$ is 2.5 mA cm^{-2} . This higher CCD, compared to NaB_3H_8 (0.8 mA cm^{-2}), suggests that introducing the neutral molecule not only increased ionic conductivity but also improved compatibility with Na. The CCD value of $\text{NaB}_3\text{H}_8\cdot\text{xNH}_3@\text{NaB}_3\text{H}_8$ was the highest in hydridoborate SSEs, suggesting excellent capability to suppress the Na dendrite formed. The GC curves of $\text{Na}/\text{NaCB}_9\text{H}_{10}/\text{Na}$ were examined at 60°C and 27°C under an applied stack pressure to ensure good interfacial contact between the SSEs and the Na anode to prevent void formation.^[53] Both cells exhibited increased overpotential during cycling, indicating the formation of an interphase or voids. The CCD of $\text{NaCB}_9\text{H}_{10}$ was investigated by the capacity control protocol with 0.2 mA h cm^{-2} at a stack pressure of 2.7 MPa . The cell was precycled at 0.2 mA cm^{-2} for 200 hours, and each cycle rested for at least two minutes. The potential decreases during the measurements when the current density reaches 1 mA cm^{-2} , indicating void formation. Hence, a current density of 0.7 mA cm^{-2} can be ascribed as the CCD value of

$\text{NaCB}_9\text{H}_{10}$. This result indicated that $\text{NaCB}_9\text{H}_{10}$ exhibits poor interfacial stability against the Na metal anode.

Beyond single-anion hydridoborates, compatibility and CCD of mixed anion-hydridoborates have also been extensively studied. The GC curve of a symmetric $\text{Na}/\text{Na}_4\text{B}_{12}\text{H}_{12}\text{B}_{10}\text{H}_{10}/\text{Na}$ cell at 60°C with a current density of 0.1 mA cm^{-2} was illustrated.^[16a] The sodium plating and stripping occurring fully reversibly and a maximum overpotential of 1.2 mV exhibit great interfacial compatibility with the Na metal anode. For $\text{Na}_2\text{BH}_4\text{NH}_2$, stability was investigated using a symmetric $\text{NaSn}/\text{Na}_2\text{BH}_4\text{NH}_2/\text{NaSn}$ cell at 90°C .^[56] The poor compatibility between Na metal and $\text{Na}_2\text{BH}_4\text{NH}_2$ led to the formation of an additional passivated interphase. The polarization voltage slightly increasing from approximately 0.06 V to 0.074 V after 500 hours at 0.1 mA cm^{-2} , indicating a stable interphase between $\text{Na}_2\text{BH}_4\text{NH}_2$ and NaSn . The CCD was determined to be 0.9 mA cm^{-2} . In the symmetric $\text{Na}/\text{Na}_4(\text{CB}_{11}\text{H}_{12})_2(\text{B}_{12}\text{H}_{12})/\text{Na}$ cell, the polarization voltage started at $\pm 8.5 \text{ mV}$ and remained stable at around $\pm 6 \text{ mV}$ for 500 hours with intervals of 30 minutes.^[57] The conductivity measured in the symmetric sodium electrode was consistent with that in the SUS electrode at 60°C . The CCD of $\text{Na}_4(\text{CB}_{11}\text{H}_{12})_2(\text{B}_{12}\text{H}_{12})$ was investigated by the capacity of 0.5 C at a stack pressure of 1.5 MPa . The polarization voltage remained stable and gradually increased with rising current density; however, a sudden voltage drop occurred when the current density reached 0.6 mA cm^{-2} , indicating that the CCD of $\text{Na}_4(\text{CB}_{11}\text{H}_{12})_2(\text{B}_{12}\text{H}_{12})$ is 0.6 mA cm^{-2} .

In the symmetric $\text{Na}/\text{Na}_2\text{B}_{20}\text{H}_{18}\cdot 4\text{Na}_2\text{B}_{12}\text{H}_{12}/\text{Na}$ cell, the overpotential during charge and discharge showed only a slight increase, remaining nearly stable at around 40 mV for 100 hours at a current density of 0.1 mA cm^{-2} , suggesting a slow parasitic reaction at the SSEs and sodium interface.^[43a] The voltage profile dropped suddenly when the current density reached 0.8 mA cm^{-2} (the CCD value is 0.8 mA cm^{-2}). For the chemical compatibility of $\text{Na}_4\text{B}_{20}\text{H}_{18}\cdot 3\text{Na}_2\text{B}_{12}\text{H}_{12}$ with metallic sodium, the voltage profiles show reversible sodium plating and stripping at a current density of 0.1 mA cm^{-2} over 100 hours at RT.^[43b] During the charging and discharging process, the polarization voltage exhibited only a slight increase from 20 to 30 mV , demonstrating good chemical compatibility between $\text{Na}_4\text{B}_{20}\text{H}_{18}\cdot 3\text{Na}_2\text{B}_{12}\text{H}_{12}$ and metallic sodium. When subjected to stepped current densities, the voltage gradually increased and suddenly dropped at a CCD of 0.4 mA cm^{-2} , which indicates the CCD value is 0.4 mA cm^{-2} . For the stability testing, the symmetric $\text{Na}/\text{Na}_3\text{B}_{24}\text{H}_{23}\cdot 5\text{Na}_2\text{B}_{12}\text{H}_{12}/\text{Na}$ cell was evaluated for compatibility.^[43c] It exhibited a stable overpotential of 12.5 mV at 0.2 mA cm^{-2} over 100 hours at 60°C (Figure 9a). After 100 hours of cycling, the impedance resistance of the $\text{Na}/\text{Na}_3\text{B}_{24}\text{H}_{23}\cdot 5\text{Na}_2\text{B}_{12}\text{H}_{12}/\text{Na}$ cell, measured by electrochemical impedance spectroscopy (EIS), showed no significant change. The CCD value of this cell in Figure 9b was 1.0 mA cm^{-2} , which is higher than that of ball-milled $\text{Na}_2\text{B}_{12}\text{H}_{12}$ (0.2 mA cm^{-2}) and ball-milled $\text{Na}_3\text{B}_{24}\text{H}_{23}$ (0.4 mA cm^{-2}). In comparison, the GC curves of $\text{Na}/\text{Na}_3\text{B}_{24}\text{H}_{23}\cdot 5\text{Na}_2\text{B}_{12}\text{H}_{12}/\text{Na}$ cell were also tested at RT. The overpotential of the $\text{Na}/\text{Na}_3\text{B}_{24}\text{H}_{23}\cdot 5\text{Na}_2\text{B}_{12}\text{H}_{12}/\text{Na}$ cell at RT increased from 80 mV to 100 mV after 100 hours of cycling, but it still maintained a CCD value of 0.7 mA cm^{-2} . A symmetric $\text{Na}/\text{Na}_4\text{B}_{36}\text{H}_{34}\cdot 7\text{Na}_2\text{B}_{12}\text{H}_{12}/\text{Na}$ cell was used to evaluate interfacial stability at 0.1 mA cm^{-2} (Figure 9c).^[43d] The voltage profile

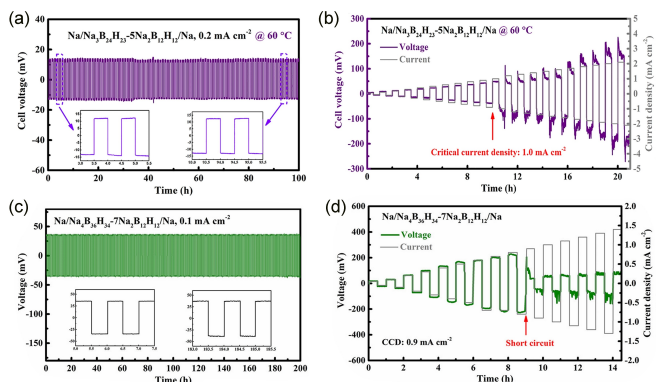


Figure 9. (a) Constant current GC curves of the $\text{Na}/\text{Na}_3\text{B}_{24}\text{H}_{23}\cdot 5\text{Na}_2\text{B}_{12}\text{H}_{12}/\text{Na}$ cells at a current density of 0.1 mA cm^{-2} with interval of 30 min and (b) stepped current GC curve of a $\text{Na}/\text{Na}_3\text{B}_{24}\text{H}_{23}\cdot 5\text{Na}_2\text{B}_{12}\text{H}_{12}/\text{Na}$ cell (reprinted with permission from ref. [43c] Copyright 2022 Elsevier B.V.), (c) Constant current GC curves of the $\text{Na}/\text{Na}_4\text{B}_{36}\text{H}_{34}\cdot 7\text{Na}_2\text{B}_{12}\text{H}_{12}/\text{Na}$ cells at a current density of 0.1 mA cm^{-2} with interval of 30 min and (d) stepped current GC curve of a $\text{Na}/\text{Na}_4\text{B}_{36}\text{H}_{34}\cdot 7\text{Na}_2\text{B}_{12}\text{H}_{12}/\text{Na}$ cell (reprinted with permission from ref. [43d] Copyright 2024 American Chemical Society).

showed no significant changes, with the overpotential only slightly increasing from 35 to 37 mV after more than 200 hours of cycling. The tested interfacial resistance also showed minimal change, which is in good agreement with the observed overpotential changes. The CCD of $\text{Na}_4\text{B}_{36}\text{H}_{34}\cdot 7\text{Na}_2\text{B}_{12}\text{H}_{12}$ (Figure 9d) was 0.9 mA cm^{-2} , higher than that of $\text{Na}_4\text{B}_{36}\text{H}_{34}$ (0.4 mA cm^{-2}), suggesting superior compatibility, stability, and dendrite suppression in $\text{Na}_4\text{B}_{36}\text{H}_{34}\cdot 7\text{Na}_2\text{B}_{12}\text{H}_{12}$ against to Na.

3.3. ASSMBs Performances

Beyond compatibility with Na metal in symmetric cells, the wettability, electrochemical stability, and application potential in ASSMBs need further investigation. The representative sodium metal batteries performances with hydridoborate SSEs are shown in Table 2. A $\text{Na}/\text{NaCB}_9\text{H}_{10}/\text{NaTi}_2(\text{PO}_4)_3$ cell was assembled using sodium metal as the anode and $\text{NaTi}_2(\text{PO}_4)_3$ (NTP) as the cathode.^[53] During discharge, the potential initially declined and then stabilized around 1.85 V . The discharge capacity of this cell was 68.1 mAh g^{-1} , which is 51% of the theoretical capacity. The Na-ball-milled $\text{NaB}_3\text{H}_8/\text{TiS}_2$ batteries were used to evaluate the electrochemical stability of NaB_3H_8 at 30°C .^[11b] The CV curves displayed multiple pairs of redox peaks in the range of 1.40 to 2.40 V with good overlap, demonstrating that Na^+ intercalation/extraction in TiS_2 was a reversible multi-step process and that NaB_3H_8 exhibits excellent stability during intercalation/extraction. In Figure 6a, as the rate increased to 1 C , the battery retained 86.0% of its capacity at 0.1 C (168.0 mAh g^{-1}). After 300 cycles, the capacity was 99.2 mAh g^{-1} , with a capacity retention of 70.9% and a coulombic efficiency close to 100% , indicating high long-term cycling stability at 1 C (Figure 10b). The curves also displayed well-overlapped, higher, and narrower redox peaks at a high temperature of 55°C , suggesting the excellent battery performance of NaB_3H_8 . Similar to NaB_3H_8 , the CV curves of $\text{NaB}_3\text{H}_8\cdot x\text{NH}_3/\text{NaB}_3\text{H}_8$ also showed multi-step intercalation/ex-

Table 2. Representative sodium metal batteries performances with hydridoborate SSEs.

Electrolytes	Batteries	T _w ^[a] /P ^[b]	O.V. ^[c]	E ^[d] /C.A.M.L. ^[e]	Rate/C ^[f]	C ^[g] /C.R. ^[h]	Ref.
NaB ₃ H ₈	Na//TiS ₂	30/N.R. ^[i]	1.4–2.4	0.8–1.2/0.61	1/141	300/71 %	[11b]
NaB ₃ H ₈ ·xNH ₃ @NaB ₃ H ₈	Na//TiS ₂	30/N.R.	1.4–2.4	1/0.53	1/232	300/90 %	[11a]
/	/	30/N.R.	1.4–2.4	1/0.53	10/54	300/90 %	[11a]
Na ₂ B ₂₀ H ₁₈ ·4Na ₂ B ₁₂ H ₁₂	Na//TiS ₂	RT/N.R.	1.5–2.7	0.4–0.5/0.75	0.1/65	100/82 %	[43a]
Na ₄ B ₂₀ H ₁₈ ·3Na ₂ B ₁₂ H ₁₂	Na//TiS ₂	RT/N.R.	1.2–2.7	0.4–0.6/0.75	0.1/38	50/92 %	[43b]
Na ₃ B ₂₄ H ₂₃ ·5Na ₂ B ₁₂ H ₁₂	Na//Na _{1/3} Fe _{1/3} Mn _{1/3} O ₂	RT/N.R.	2–4.2	0.4–0.6/1.2	0.1/51	50/87 %	[43c]
/	/	60/N.R.	2–4.2	0.4–0.6/1.2	0.1/62	100/84 %	[43c]
Na ₄ B ₃₆ H ₃₄ ·7Na ₂ B ₁₂ H ₁₂	Na//Na ₃ V ₂ (PO ₄) ₂ O ₂ F	RT/N.R.	2.5–4.5	0.4–0.6/1.2	0.1/71	100/86 %	[43d]
Na ₃ NH ₂ B ₁₂ H ₁₂	Na//TiS ₂	80/N.R.	1–2.4	1/0.6	0.1/146	200/53 %	[36]
Na ₈ (B ₁₀ H ₁₀)(B ₁₂ H ₁₂) ₃	Na//TiS ₂	30/N.R.	1–2.9	N.R./1.71	0.02/254	11/85 %	[54]
Na ₄ (B ₁₂ H ₁₂)(B ₁₀ H ₁₀)	Na//NaCrO ₂	60/N.R.	2–3.25	0.5/1.2	0.2/80	250/85 %	[34]
Na ₄ (B ₁₂ H ₁₂)(B ₁₀ H ₁₀)	NaSn//NaCrO ₂	30/350	2.1–3.4	0.5/7.7	0.5/118	100/93 %	[58]
Na ₄ (CB ₁₁ H ₁₂) ₂ (B ₁₂ H ₁₂)	Na//Na ₃ (VOPO ₄) ₂ F	RT/3.2	2.5–4.15	0.6/1.1	0.2/99	800/76 %	[33a]
Na ₂ (BH ₄)(NH ₂)	NaSn//TiS ₂	90/N.R.	1.2–2.4	N.R.	0.08/160	43/29 %	[56]

[a] Working temperature. [b] Pressure. [c] Operation voltage. [d] Electrolyte thickness. [e] Cathode active material mass (mg cm⁻¹). [f] Capacities. [g] Cycles. [h] Capacity retention. [i] Not reported.

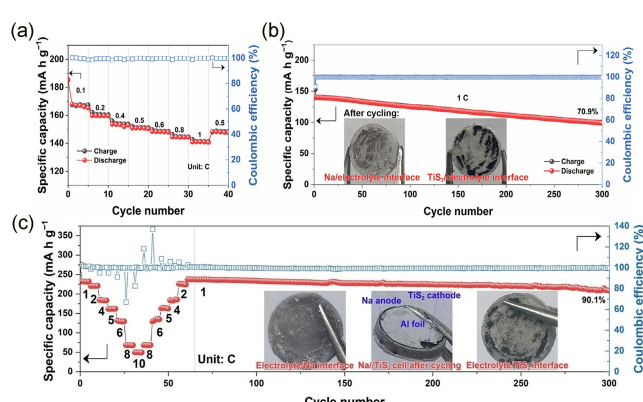


Figure 10. (a) Rate performance at current density from 0.1 to 1 C and (b) cycling performance at 1 C of Na/ball-milled NaB₃H₈/TiS₂ cell (reprinted with permission from ref. [11b] Copyright 2024 Wiley-VCH Verlag GmbH & Co. KGaA, Weinheim), (c) rate and cycling performance from 1 C to 10 C and subsequent cycling at 1 C of Na/B₃H₈·xNH₃@NaB₃H₈/TiS₂ cell (reprinted with permission from ref. [11a] Copyright 2024 Wiley-VCH Verlag GmbH & Co. KGaA, Weinheim), insets in (b) and (c): photographs of the interfaces after cycling.

traction with good overlap, indicating stable cycling performance.^[11a] The Na//NaB₃H₈·xNH₃@NaB₃H₈/TiS₂ battery showed a first discharge capacity of 237.2 mAh g⁻¹ at 1 C (Figure 10c). After 240 cycles, the capacity retention was 90.1%, with a stable Coulombic efficiency close to 100%. The capacity retention and coulombic efficiency could be comparable to those of a liquid Na//TiS₂ battery previously reported. Additionally, the battery demonstrated good cycling stability at 5 C with a capacity of 135.0 mAh g⁻¹ and a retention of 86.2%, and at 10 C with a capacity of 33.6 mAh g⁻¹ and a retention of 62.1%. Most notably, the superior long-life cycling stability at 5 and 10 C is rarely reported in ASSMBs.

The ASSBs performance of Na₃NH₂B₁₂H₁₂ was studied by mixing with 50 wt% ratio of active material TiS₂ to make a positive electrode layer. Assembled TiS₂Na₃NH₂B₁₂H₁₂/Na₃NH₂B₁₂H₁₂/Na (Figure 11a) cell exhibits a discharge capacity of 146 mAh g⁻¹ in the second cycle and Coulombic efficiency keeps approximately 100% at 70 °C and 0.1 C.^[36] It showed a high capacity retention of 102 mAh g⁻¹ after 100 cycles and 77 mAh g⁻¹ over 200 cycles. The XRD results of SSEs show a small proportion of Na₂B₁₂H₁₂ increased may come from partial decomposition of Na₃NH₂B₁₂H₁₂. The results indicate Na₃NH₂B₁₂H₁₂ decomposition is very slow and can be the promising SSEs. For Na₂BH₄NH₂, CV curves showed two redox pairs, confirming Na⁺ intercalation/extraction into TiS₂.^[56]

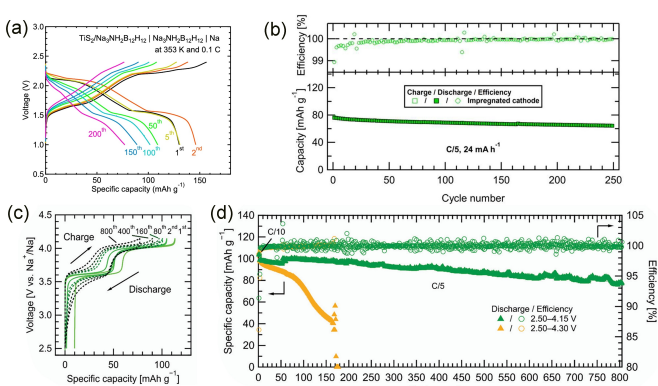


Figure 11. (a) Discharge/charge curves over 200 cycles of TiS₂/Na₃NH₂B₁₂H₁₂/Na₃NH₂B₁₂H₁₂/Na cell (reprinted with permission from ref. [36] Copyright 2018 Elsevier B.V.), (b) Discharge/charge curves over 250 cycles of Na/Na₄(B₁₂H₁₂)(B₁₀H₁₀)/NaCrO₂ cell (reprinted with permission from ref. [34] Copyright 2017 The Royal Society of Chemistry), (c) discharge/charge curves at C/10 with voltage of 4.15 V, and (d) cycling performance of Na₃(VOPO₄)₂F/Na₄(CB₁₁H₁₂)₂(B₁₂H₁₂)/Na cell (reprinted with permission from ref. [33a] Copyright 2020 The Royal Society of Chemistry).

Although the first discharge capacity was 147.8 mAh g^{-1} , the capacity dropped to 27.0% of its initial value after 15 cycles. This unfavorable cycling performance suggests the formation of additional passivation layers between TiS_2 and $\text{Na}_2\text{BH}_4\text{NH}_2$ or a reaction between Na metal and $\text{Na}_2\text{BH}_4\text{NH}_2$. A composite positive electrode by mixing TiS_2 and $\text{Na}_2\text{B}_{10}\text{H}_{10}-3\text{Na}_2\text{B}_{12}\text{H}_{12}$ with a 2:3 mass ratio has investigated the performance of $\text{Na}_2\text{B}_{10}\text{H}_{10}-3\text{Na}_2\text{B}_{12}\text{H}_{12}$.^[54] The battery was tested at 30°C and 0.02 C , and the discharge/charge profile exhibited two voltage plateaus at 2.1–2.3 V and 1.2–1.7 V. This can be attributed to the multi-step intercalation of sodium into TiS_2 , which varies with sodium stoichiometry. After 11 cycles, the discharge capacity was 216 mAh g^{-1} , which exhibits a high discharge capacity retention ratio above 91% from the second discharge capacity. The $\text{Na}/\text{Na}_4(\text{B}_{12}\text{H}_{12})(\text{B}_{10}\text{H}_{10})/\text{NaCrO}_2$ cell (Figure 11b) shows a discharge capacity of 88 mAh g^{-1} and coulombic efficiency of 89%.^[33a] Coulombic efficiency increases to 99% and is retained at 94.6% after 20 cycles at $\text{C}/20$. Rate tests indicate the cell can be cycled at $\text{C}/5$ with very little capacity loss. After 250 cycles at $\text{C}/5$, the cell capacity is retained at 85% with a Coulombic efficiency of 99.5%, confirming the high stability of the system. When using NaCrO_2 as the electrode, the first discharge capacity of $\text{Na}/\text{Na}_4(\text{CB}_{11}\text{H}_{12})_2(\text{B}_{12}\text{H}_{12})/\text{NaCrO}_2$ is 108.6 mAh g^{-1} at $\text{C}/20$.^[57] The specific capacity retention is 94%, and Coulombic efficiency is raised up to 99%. Besides, the discharge capacity of cells was also investigated based on $\text{Na}_3(\text{VOPO}_4)_2\text{F}$ as cathode, $\text{Na}_4(\text{CB}_{11}\text{H}_{12})_2(\text{B}_{12}\text{H}_{12})$ as the SSEs, and sodium metal as anode. The discharge/charge curves and cycling performance are shown in Figure 11c and Figure 11d. The operation voltage can reach up to 4.15 V, and the discharge capacity was 104 mAh g^{-1} at 0.1 C and 99 mAh g^{-1} at $\text{C}/5$.^[33a] It also demonstrated excellent capacity retention of 76% and energy retention of 78% after 800 cycles at $\text{C}/5$ in Figure 11d, indicating the significant application prospects in ASSMBs.

The all-solid-state $\text{Na}/\text{Na}_2\text{B}_{20}\text{H}_{18}\cdot4\text{Na}_2\text{B}_{12}\text{H}_{12}/\text{TiS}_2$ cell was used to evaluate battery performance.^[43a] The cell delivered a discharge capacity of 64.8 mAh g^{-1} in the first cycle, with a coulombic efficiency greater than 99.2%, and retained 82% of its discharge capacity after 100 cycles. The charge/discharge behavior of the $\text{Na}/\text{Na}_2\text{B}_{20}\text{H}_{18}\cdot3\text{Na}_2\text{B}_{12}\text{H}_{12}/\text{TiS}_2$ cell was evaluated using CV at RT.^[43b] The redox peaks in the CV curves indicate the multi-step nature of the layered TiS_2 . The cell exhibited a discharge capacity of 38.1 mAh g^{-1} at 0.1 C in the first cycle. The Coulombic efficiency was nearly 100%, and the capacity retention was 92% after 50 cycles, demonstrating the excellent cycling stability of $\text{Na}_2\text{B}_{20}\text{H}_{18}\cdot3\text{Na}_2\text{B}_{12}\text{H}_{12}$. Additionally, the cell showed good rate performance across a range of rates from $\text{C}/20$ to $\text{C}/2$, with specific capacities of 58.1 mAh g^{-1} at $\text{C}/20$ and 18.6 mAh g^{-1} at $\text{C}/2$. When the current density was returned to $\text{C}/20$, the specific capacity was 55.7 mAh g^{-1} . $\text{Na}_3\text{B}_{24}\text{H}_{23}$ exhibits an ultra-high electrochemical stability window (ESW) of 6.7 V vs. Na^+/Na , which far exceeds that of $\text{Na}_2\text{B}_{12}\text{H}_{12}$ (4.2 V vs. Na^+/Na). A galvanostatic cycling performance and long-term cycling performance of $\text{Na}[\text{Ni}_{1/3}\text{Fe}_{1/3}\text{Mn}_{1/3}]\text{O}_2/\text{Na}_3\text{B}_{24}\text{H}_{23}\cdot5\text{Na}_2\text{B}_{12}\text{H}_{12}/\text{Na}$ cell was assembled and tested at 60°C and RT within a voltage range of 2.0–4.2 V. At 60°C (Figure 12a and Figure 12b), the cell delivered a discharge capacity of 62.3 mAh g^{-1} at 0.1 C , with a

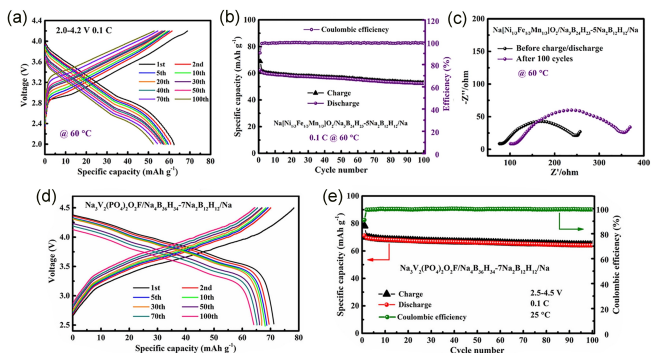


Figure 12. (a) Galvanostatic cycling performance, (b) long-term cycling performance, (c) EIS spectra before and after cycling of the $\text{Na}[\text{Ni}_{1/3}\text{Fe}_{1/3}\text{Mn}_{1/3}]\text{O}_2/\text{Na}_3\text{B}_{24}\text{H}_{23}\cdot5\text{Na}_2\text{B}_{12}\text{H}_{12}/\text{Na}$ cells (reprinted with permission from ref. [43c] Copyright 2022 Elsevier B.V.), (d) Charge–discharge voltage profiles and (e) long-term cycling performance of $\text{Na}_3\text{V}_2(\text{PO}_4)_2\text{O}_2\text{F}/\text{Na}_4\text{B}_{36}\text{H}_{24}\cdot7\text{Na}_2\text{B}_{12}\text{H}_{12}/\text{Na}$ cell (reprinted with permission from ref. [43d] Copyright 2024 American Chemical Society).

Coulombic efficiency of 89% in the first cycle. As cycling progressed, the Coulombic efficiency quickly increased to nearly 100%, with a discharge capacity of 52.3 mAh g^{-1} (84% retention) after 100 cycles.

The EIS spectra before and after cycling are shown in Figure 12c. It can be seen that the EIS data were minor changes. At RT, the cell exhibited larger polarization and smaller discharge capacities, with an initial discharge capacity of 51.2 mAh g^{-1} and 87% retention after 50 cycles. At both temperatures, the $\text{Na}[\text{Ni}_{1/3}\text{Fe}_{1/3}\text{Mn}_{1/3}]\text{O}_2/\text{Na}_3\text{B}_{24}\text{H}_{23}\cdot5\text{Na}_2\text{B}_{12}\text{H}_{12}/\text{Na}$ cell demonstrated excellent cycling stability and good rate performance. Besides, in lower voltage operation, the $\text{TiS}_2/\text{Na}_3\text{B}_{24}\text{H}_{23}\cdot5\text{Na}_2\text{B}_{12}\text{H}_{12}/\text{Na}$ cell showed a high discharge capacity of 171.4 mAh g^{-1} at 0.1 C , remaining stable over 100 cycles. For $\text{Na}_4\text{B}_{36}\text{H}_{34}\cdot7\text{Na}_2\text{B}_{12}\text{H}_{12}$, the ESW was as high as 6.9 V. To investigate its performance in a high-voltage system, a $\text{Na}_3\text{V}_2(\text{PO}_4)_2\text{O}_2\text{F}/\text{Na}_4\text{B}_{36}\text{H}_{34}\cdot7\text{Na}_2\text{B}_{12}\text{H}_{12}/\text{Na}$ cell was tested between 2.5 and 4.5 V at RT and the galvanostatic cycling performance and long-term cycling performance are shown in Figure 12d and Figure 12e. The cell delivered a discharge capacity of 71.2 mAh g^{-1} in the first cycle, with a capacity retention of 85.8% and a coulombic efficiency of over 99% after 100 cycles at 0.1 C . Additionally, the cell based $\text{Na}_3\text{V}_2(\text{PO}_4)_2\text{O}_2\text{F}$ as the electrode demonstrated good rate performance. These results confirm the excellent compatibility of $\text{Na}_4\text{B}_{36}\text{H}_{34}\cdot7\text{Na}_2\text{B}_{12}\text{H}_{12}$ in 4 V-class ASSMBs.

The hydridoborate-based Na-ion compounds exhibit excellent performance for application in ASSMBs. The $\text{NaB}_3\text{H}_8\cdot\text{xNH}_3@\text{NaB}_3\text{H}_8$ exhibited excellent capability and interfacial stability against Na metal and the highest CCD value of 2.5 mA cm^{-2} in hydridoborate-based Na-ion compounds. The $\text{Na}/\text{NaB}_3\text{H}_8\cdot\text{xNH}_3@\text{NaB}_3\text{H}_8/\text{TiS}_2$ battery displayed capacity 232.4 mAh g^{-1} (97.2% of theoretical capacity) and superior long-life stability at 1 C . At the same time, this battery showed long-term cycling at 10 C , rarely reported in ASSMB. $\text{Na}_4\text{B}_{36}\text{H}_{34}$ exhibited the widest ESW beyond 6.9 V among hydridoborate-based Na-ion. The operation voltage of $\text{Na}/\text{Na}_4\text{B}_{36}\text{H}_{34}\cdot7\text{Na}_2\text{B}_{12}\text{H}_{12}/\text{Na}_3\text{V}_2(\text{PO}_4)_2\text{O}_2\text{F}$ cell was 2.5 and 4.5 V, and the cell exhibited

discharge capacity of 71.2 mAh g^{-1} and good cycling stability with capacity retention of 85.8% after 100 cycles.

4. Representative Synthetic Approaches for Hydridoborate SSEs.

Presently, the major disadvantage of hydridoborates on the way to ASSMBs is their high cost and scarce commercial sources. It can be seen from the price information in Katchem that except NaBH_4 (1 kg/ 374 €), the prices of *nido/closo*-borates ($\text{NaB}_{11}\text{H}_{14}$: 10 g/ 3476 €, $\text{NaCB}_9\text{H}_{10}$: 50 g/ 19374 €, $\text{NaCB}_{11}\text{H}_{12}$: 50 g/ 20186 €, $\text{Na}_2\text{B}_{10}\text{H}_{10}$: 100 g/ 14409 €, and $\text{Na}_2\text{B}_{12}\text{H}_{12}$: 1 kg/ 12051 €) are very high that seriously limits the application. $\text{Na}_2\text{CB}_{11}\text{H}_{12}\text{CB}_9\text{H}_{10}$, which exhibits highest ionic conductivity for hydridoborates to date, is sold for about 395 €/g. The price of $\text{NaB}_3\text{H}_8 \cdot 3 \text{ C}_4\text{H}_8\text{O}_2$ is 10 g/ 555 €, and solvent-free NaB_3H_8 is not commercially available. The high yield to synthesize highly ionic conductivity hydridoborates from inexpensive bulk chemicals is of great interest.

Hansen et al. reported some methods in the review to synthesize $\text{B}_{10}\text{H}_{10}^{2-}$ and $\text{B}_{12}\text{H}_{12}^{2-}$.^[59] In addition to these approaches, there are other methods to synthesize $\text{Na}_2\text{B}_{12}\text{H}_{12}$. The dry borax with sodium (and aluminum) metal can synthesize $\text{Na}_2\text{B}_{12}\text{H}_{12}$ at 600°C under hydrogen gas at 3 bar.^[60] It also can be synthesized by $\text{NaNH}_2/\text{MBH}_4$ with $\text{B}_{10}\text{H}_{14}$.^[61] Up to date, the main approaches reported methods to synthesis *closo/nido*-hydridoborates were based on multi-step reactions and each of them has relatively low yields.

Based on this situation, our group has done a series of related work on the synthesis of hydridoborates, and the corresponding synthesis route scheme is shown in Figure 13.^[62-66] Solvent-free NaB_3H_8 can be obtained using NaBH_4 and $\text{THF}\cdot\text{BH}_3$ with a reaction time of 66 h.^[64] The longer time is ascribed to the poor solubility of NaBH_4 in THF. The purity is more than 95%, with a 43% isolated yield. Solvent-free $\text{NaB}_{11}\text{H}_{14}$ were also obtained with 65% yields at reactions of NaBH_4 and dimethyl sulfide borane ($(\text{CH}_3)_2\text{S}\cdot\text{BH}_3$) with a molar ratio of 1:10 in 1,4-dioxane at 90°C for 5 days.^[65] The *nido*- $\text{B}_{11}\text{H}_{14}^-$ anion can be important precursor for the synthesis of $\text{NaCB}_{11}\text{H}_{12}$ and $\text{Na}_2\text{B}_{12}\text{H}_{12}$. We obtained $\text{Na}_2\text{B}_{12}\text{H}_{12}$ through $\text{NaB}_{11}\text{H}_{14}$ reacting with NaB_3H_8 in diglyme at 140°C with a 1:1 molar ratio for 40 h.^[65] The yield can reach up to 80%. The 1:1:3:3 molar ratio of $\text{NaB}_{11}\text{H}_{14}$ to NaHMDS to NaH to CF_3SiMe_3 can effectively prepare solvent-free 68% yields.^[63] It is worth noting that the NaB_3H_8 , $\text{NaB}_{11}\text{H}_{14}$, $\text{Na}_2\text{B}_{12}\text{H}_{12}$, and $\text{NaCB}_{11}\text{H}_{12}$ have been synthesized without using the highly reactive and hazardous B_2H_6 , B_5H_9 , and $\text{B}_{10}\text{H}_{14}$. Based on $\text{B}_{10}\text{H}_{14}$ as the precursor, we developed the methods to synthetic $\text{NaB}_9\text{H}_{14}$ (yet reported), $\text{Na}_2\text{B}_{10}\text{H}_{14}$, and $\text{NaCB}_9\text{H}_{10}$.^[62, 66] The synthesis method of $[\text{Et}_4\text{N}][\text{CB}_9\text{H}_{10}]$ is facile, rapid, and scalable (37 g), and its overall yield is up to 80%.^[62] It can almost completely convert into $\text{NaCB}_9\text{H}_{10}$ by ion exchange. The disadvantage of this reaction is that the highly toxic $\text{B}_{10}\text{H}_{14}$ is used as a raw material in the synthesis process. We have been working on the exploration of more inexpensive bulk chemicals and more efficiently synthesizing related borane compounds, and significant progress has been made in the synthesis of hydridoborates.

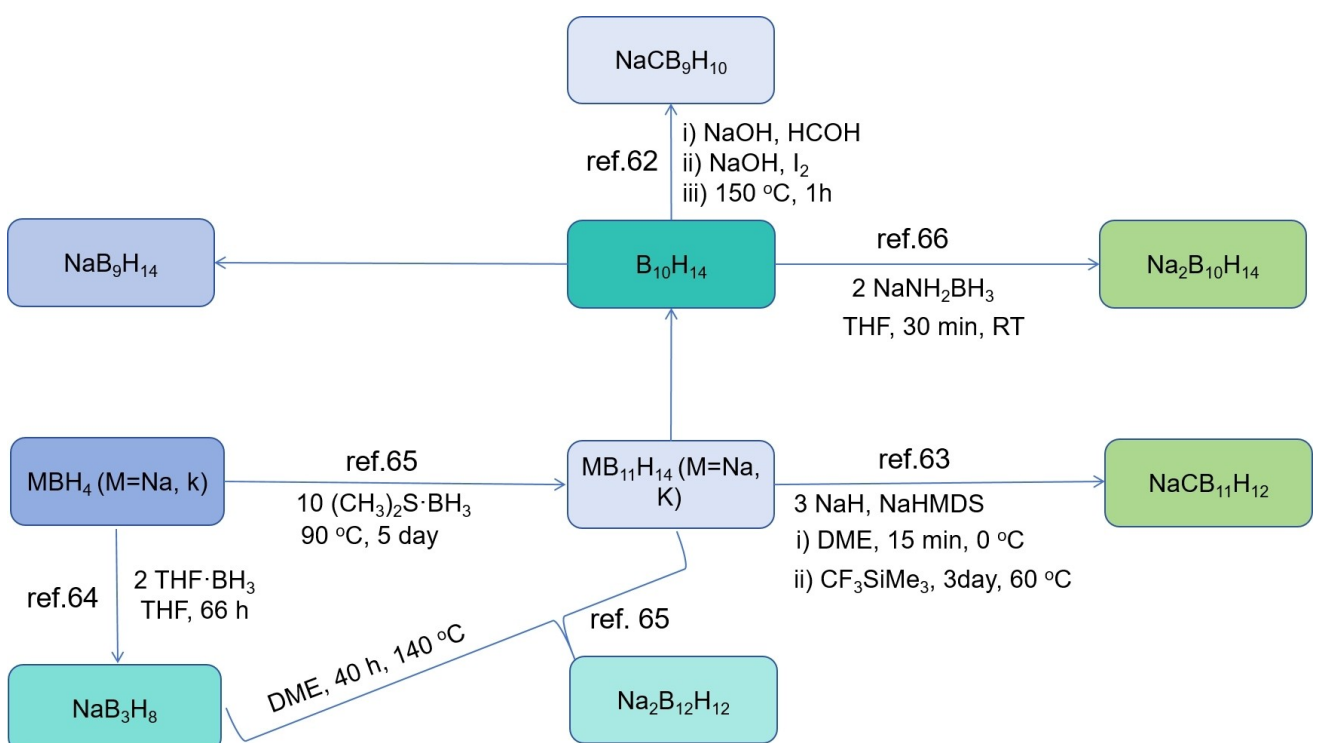


Figure 13. (a) Synthesis routes for several hydridoborates starting from the $\text{NaBH}_4/\text{KBH}_4$ by our group. The details experimental procedure could found in reference paper.

5. Summary and Outlook

The hydridoborate-based Na-ion compounds exhibit excellent performance for application in ASSMBs. This review summarizes various hydridoborate-based Na-ion compounds of ionic conductivity, thermal stability, ESW, CCD, stability against Na metal, and dendrite prevention stability for their application in ASSMBs. We also overview recent advances in the synthesis of hydridoborate compounds. The *closo*-polyborate dianions and polyhedral(carba)borate anions appeared as the most stable boranes. Most of these hydridoborates exhibit excellent stability against the Na metal well-suited for SSEs, particularly in mixed anion systems. Among them, $\text{Na}_2\text{CB}_9\text{H}_{10}\text{CB}_{11}\text{H}_{12}$ displayed Na^+ conductivity of 10^{-2} Scm^{-1} at RT, comparable to liquid electrolytes. The $\text{NaB}_3\text{H}_8 \cdot x\text{NH}_3 @ \text{NaB}_3\text{H}_8$ battery exhibit a high CCD of 2.5 mA cm^{-2} , a high capacity of 232.4 mAh g^{-1} at 1 C (97.2% of theoretical capacity), and long-term stability could be comparable to liquid Na/TiS₂ battery previously reported. The superior long-life cycling operation at 10 C has rarely been reported in ASSMBs. The ESW of $\text{Na}_4\text{B}_{36}\text{H}_{34} \cdot 7\text{Na}_2\text{B}_{12}\text{H}_{12}$ was as high as 6.9 V, and the $\text{Na}_3\text{V}_2(\text{PO}_4)_2\text{O}_2\text{F} / \text{Na}_4\text{B}_{36}\text{H}_{34} \cdot 7\text{Na}_2\text{B}_{12}\text{H}_{12}/\text{Na}$ cell operation at 4.5 V that also exhibit excellent cycling stability.

Some challenges remain for use in the commercialization of ASSMBs. The high price significantly slows down the application of borohydride in ASSMBs, and thus, exploring more environmentally friendly, inexpensive, highly effective synthesis methods is necessary. The compatibility of high ionic conductivity, high thermal stability, CCD, high rate, high ESW, low price, and high theoretical capacity cathode are rarely reported. Besides, the improvement of the ionic conductivity of hydridoborates has been successfully applied by incorporating neutral ligands (NH_3 , CH_3NH_2 , or NH_3BH_3) into the LiBH_4 , the introduction of corresponding neutral molecules into hydridoborate-based Na-ion was rarely reported. The battery studies are usually based on TiS₂ as cathodes because of the stability of these electrolytes. The active material mass loading also remains relatively low (< 5 mg cm⁻²). It is of great significance to synthesize hydridoborate compounds with high ESW. We believe that hydridoborate compounds hold significant potential for commercial ASSMB applications.

Acknowledgements

This work was supported by the National Natural Science Foundation of China (Grant Nos. U18042532, U23A2078, and 22171246).

Conflict of Interests

The authors declare no conflict of interest.

Keywords: Hydridoborates · Solid-state electrolytes · All-solid-state sodium batteries · Interface

- [1] a) J. W. Choi, D. Aurbach, *Nat. Rev. Mater.* **2016**, *1*, 16013; b) J. Xie, S.-Y. Sun, X. Chen, L.-P. Hou, B.-Q. Li, H.-J. Peng, J.-Q. Huang, X.-Q. Zhang, Q. Zhang, *Angew. Chem. Int. Ed.* **2022**, *61*, e202204776; c) J. Hu, Z. Yao, K. Chen, C. Li, *Energy Storage Mater.* **2020**, *28*, 37–46; d) X. Chen, S. Dou, W. Li, D. Liu, Y. Zhang, Y. Zhao, Y. Li, J. Zhao, X. Zhang, *Chem. Commun.* **2020**, *56*, 5018–5021; e) C. Hu, Y. Shen, M. Shen, X. Liu, H. Chen, C. Liu, T. Kang, F. Jin, L. Li, J. Li, Y. Li, N. Zhao, X. Guo, W. Lu, B. Hu, L. Chen, *J. Am. Chem. Soc.* **2020**, *142*, 18035–18041.
- [2] C. Vaalma, D. Buchholz, M. Weil, S. Passerini, *Nat. Rev. Mater.* **2018**, *3*, 18013.
- [3] a) K. B. Hueso, M. Armand, T. Rojo, *Energy Environ. Sci.* **2013**, *6*, 734–749; b) S. Paarmann, M. Schreiber, A. Chahbaz, F. Hildenbrand, G. Stahl, M. Rogge, P. Dechent, O. Queisser, S. D. Frankl, P. Morales Torricos, Y. Lu, N. I. Nikolov, M. Kateri, D. U. Sauer, M. A. Danzer, T. Wetzel, C. Endisch, M. Lienkamp, A. Jossen, M. Lewerenz, *Batteries Supercaps* **2024**, *7*, e202300594; c) M. Fichtner, *Batteries & Supercaps* **2022**, *5*, e202100224.
- [4] a) D. W. McOwen, S. Xu, Y. Gong, Y. Wen, G. L. Godbey, J. E. Gritton, T. R. Hamann, J. Dai, G. T. Hitz, L. Hu, E. D. Wachsman, *Adv. Mater.* **2018**, *30*, 1707132; b) Y. Kato, S. Hori, T. Saito, K. Suzuki, M. Hirayama, A. Mitsui, M. Yonemura, H. Iba, R. Kanno, *Nat. Energy* **2016**, *1*, 16030; c) P. Stüble, C. Müller, N. Bohn, M. Müller, A. Hofmann, T. Alkay, J. Clemens, A. Koeppe, S. Kolli, D. Rajagopal, H. Geßwein, W. Schabel, P. Scharfer, M. Selzer, J. R. Binder, A. Smith, *Batteries Supercaps* **2024** e202400406; d) A. Liu, S. Lu, X. Wu, *Batteries Supercaps* **2024**, e202400290.
- [5] a) J. Janek, W. G. Zeier, *Nat. Energy* **2016**, *1*, 16141; b) D. Lin, Y. Liu, Y. Cui, *Nat. Nanotechnol.* **2017**, *12*, 194–206; c) X. Yang, K. R. Adair, X. Gao, X. Sun, *Energy Environ. Sci.* **2021**, *14*, 643–671; d) A. Manthiram, X. Yu, S. Wang, *Nat. Rev. Mater.* **2017**, *2*, 16103; e) J. M. Tarascon, M. Armand, *Nature* **2001**, *414*, 359–367.
- [6] a) X. Yu, A. Manthiram, *Joule* **2017**, *1*, 453–462; b) Y. Lu, L. Li, Q. Zhang, Z. Niu, J. Chen, *Joule* **2018**, *2*, 1747–1770; c) L. Duchêne, A. Remhof, H. Hagemann, C. Battaglia, *Energy Storage Mater.* **2020**, *25*, 782–794; d) Y. Lu, H. M. Chang, K. P. Birke, *Batteries Supercaps* **2024**, e202400268; e) S. Qian, H. Chen, Z. Wu, D. Li, X. Liu, Y. Tang, S. Zhang, *Batteries & Supercaps* **2021**, *4*, 39–59; f) Y. Fang, Y. Yan, X. Wang, Z. Zhang, L. Tian, S. Lu, B. Liang, Y. Yao, D. Q. Tan, S. Huang, T. Tao, *Batteries Supercaps* **2024**, e202400121.
- [7] a) B. Lee, E. Paek, D. Mitlin, S. W. Lee, *Chem. Rev.* **2019**, *119*, 5416–5460; b) W. Xia, Y. Zhao, F. Zhao, K. Adair, R. Zhao, S. Li, R. Zou, Y. Zhao, X. Sun, *Chem. Rev.* **2022**, *122*, 3763–3819.
- [8] a) W. Hou, X. Guo, X. Shen, K. Amine, H. Yu, J. Lu, *Nano Energy* **2018**, *52*, 279–291; b) A. Hayashi, K. Noi, A. Sakuda, M. Tatsumisago, *Nat. Commun.* **2012**, *3*, 856.
- [9] a) V. St-Onge, S. Rochon, J.-C. Daigle, A. Soldéa, J. P. Claverie, *Angew. Chem. Int. Ed.* **2021**, *60*, 25897–25904; b) W. Lyu, X. Yu, Y. Lv, A. M. Rao, J. Zhou, B. Lu, *Adv. Mater.* **2024**, *36*, 2305795.
- [10] a) Y. Hu, J. Fu, J. Xu, J. Luo, F. Zhao, H. Su, Y. Liu, X. Lin, W. Li, J. T. Kim, X. Hao, X. Yao, Y. Sun, J. Ma, H. Ren, M. Yang, Y. Huang, X. Sun, *Matter* **2024**, *7*, 1018–1034; b) J. Park, J. P. Son, W. Ko, J.-S. Kim, Y. Choi, H. Kim, H. Kwak, D.-H. Seo, J. Kim, Y. S. Jung, *ACS Energy Lett.* **2022**, *7*, 3293–3301.
- [11] a) P. Qiu, X. Chen, W. Zhang, G. Zhang, Y. Zhang, Z. Lu, Y. Wu, X. Chen, *Angew. Chem. Int. Ed.* **2024**, *63*, e202401480; b) X.-W. Chen, J.-X. Kang, Z.-H. Fan, N. Zhang, W.-Y. Zhang, G.-G. Zhang, A.-Q. Zhu, Z.-W. Lu, P. Qiu, Y. Wu, X. Chen, *Small* **2024**, *20*, 2401439.
- [12] a) J.-Y. Liang, X.-D. Zhang, X.-X. Zeng, M. Yan, Y.-X. Yin, S. Xin, W.-P. Wang, X.-W. Wu, J.-L. Shi, L.-J. Wan, Y.-G. Guo, *Angew. Chem. Int. Ed.* **2020**, *59*, 6585–6589; b) M. R. Busche, T. Drossel, T. Leichtweiss, D. A. Weber, M. Falk, M. Schneider, M.-L. Reich, H. Sommer, P. Adelhelm, J. Janek, *Nat. Chem.* **2016**, *8*, 426–434; c) T. Wei, Y. Gong, X. Zhao, K. Huang, *Adv. Funct. Mater.* **2014**, *24*, 5380–5384; d) Y. Li, M. Li, Z. Sun, Q. Ni, H. Jin, Y. Zhao, *Energy Storage Mater.* **2023**, *56*, 582–599.
- [13] a) Z. Yu, S.-L. Shang, J.-H. Seo, D. Wang, X. Luo, Q. Huang, S. Chen, J. Lu, X. Li, Z.-K. Liu, D. Wang, *Adv. Mater.* **2017**, *29*, 1605561; b) S. Wenzel, T. Leichtweiss, D. A. Weber, J. Sann, W. G. Zeier, J. Janek, *ACS Appl. Mater. Interfaces* **2016**, *8*, 28216–28224; c) W. D. Richards, T. Tsujimura, L. J. Miara, Y. Wang, J. C. Kim, S. P. Ong, I. Uechi, N. Suzuki, G. Ceder, *Nat. Commun.* **2016**, *7*, 11009; d) M. Duchardt, U. Ruschewitz, S. Adams, S. Dehnen, B. Roling, *Angew. Chem. Int. Ed.* **2018**, *57*, 1351–1355.
- [14] a) D. Zhou, R. Liu, J. Zhang, X. Qi, Y.-B. He, B. Li, Q.-H. Yang, Y.-S. Hu, F. Kang, *Nano Energy* **2017**, *33*, 45–54; b) Y. Yao, Z. Wei, H. Wang, H. Huang, Y. Jiang, X. Wu, X. Yao, Z.-S. Wu, Y. Yu, *Adv. Energy Mater.* **2020**, *10*, 1903698; c) H. M. Law, J. Yu, S. C. T. Kwok, G. Zhou, M. J. Robson, J. Wu, F. Ciucci, *Energy Storage Mater.* **2022**, *46*, 182–191.

- [15] L. Wang, Z. Song, X. Lou, Y. Chen, T. Wang, Z. Wang, H. Chen, W. Yin, M. Avdeev, W. H. Kan, B. Hu, W. Luo, *Small* **2024**, *20*, 2400195.
- [16] a) L. Duchêne, R. S. Kühnel, D. Rentsch, A. Remhof, H. Hagemann, C. Battaglia, *Chem. Commun.* **2017**, *53*, 4195–4198; b) Y. Sadikin, M. Brighi, P. Schouwink, R. Černý, *Adv. Energy Mater.* **2015**, *5*, 1501016; c) H. Liu, X. Zhou, M. Ye, J. Shen, *Electrochem. Energy Rev.* **2023**, *6*, 31.
- [17] A. N. Dey, J. Miller, *J. Electrochem. Soc.* **1979**, *126*, 1445.
- [18] M. Matsuo, Y. Nakamori, S. I. Orimo, H. Maekawa, H. Takamura, *Appl. Phys. Lett.* **2007**, *91*, 224103.
- [19] M. Paskevicius, L. H. Jepsen, P. Schouwink, R. Černý, D. B. Ravnsbæk, Y. Filinchuk, M. Dornheim, F. Besenbacher, T. R. Jensen, *Chem. Soc. Rev.* **2017**, *46*, 1565–1634.
- [20] Z. Lu, F. Ciucci, *Chem. Mater.* **2017**, *29*, 9308–9319.
- [21] a) Y. Filinchuk, H. Hagemann, *Eur. J. Inorg. Chem.* **2008**, *2008*, 3127–3133; b) M. Matsuo, H. Oguchi, T. Sato, H. Takamura, E. Tsuchida, T. Ikeshoji, S. I. Orimo, *J. Alloys Compd.* **2013**, *580*, S98–S101.
- [22] a) H. Wu, W. S. Tang, V. Stavila, W. Zhou, J. J. Rush, T. J. Udoovic, *J. Phys. Chem. C* **2015**, *119*, 6481–6487; b) C. Zhou, J. B. Grinderslev, L. N. Skov, M. Jørgensen, Y. Li, J. Skibsted, Y. Yan, T. R. Jensen, *J. Mater. Chem. A* **2022**, *10*, 16137–16151.
- [23] L. M. de Kort, V. Gulino, P. E. de Jongh, P. Ngene, *J. Alloys Compd.* **2022**, *901*, 163474.
- [24] Y. Filinchuk, D. Chernyshov, A. Nevidomskyy, V. Dmitriev, *Angew. Chem. Int. Ed.* **2008**, *47*, 529–532.
- [25] Y. Pang, Y. Liu, J. Yang, S. Zheng, C. Wang, *Mater. Today Nano* **2022**, *18*, 100194.
- [26] T. J. Udoovic, M. Matsuo, W. S. Tang, H. Wu, V. Stavila, A. V. Solonin, R. V. Skoryunov, O. A. Babanova, A. V. Skripov, J. J. Rush, A. Unemoto, H. Takamura, S.-I. Orimo, *Adv. Mater.* **2014**, *26*, 7622–7626.
- [27] T. J. Udoovic, M. Matsuo, A. Unemoto, N. Verdal, V. Stavila, A. V. Skripov, J. J. Rush, H. Takamura, S.-I. Orimo, *Chem. Commun.* **2014**, *50*, 3750–3752.
- [28] a) W. S. Tang, M. Matsuo, H. Wu, V. Stavila, W. Zhou, A. A. Talin, A. V. Solonin, R. V. Skoryunov, O. A. Babanova, A. V. Skripov, A. Unemoto, S.-I. Orimo, T. J. Udoovic, *Adv. Energy Mater.* **2016**, *6*, 1502237; b) W. S. Tang, A. Unemoto, W. Zhou, V. Stavila, M. Matsuo, H. Wu, S.-I. Orimo, T. J. Udoovic, *Energy Environ. Sci.* **2015**, *8*, 3637–3645.
- [29] W. S. Tang, M. Dimitrievska, V. Stavila, W. Zhou, H. Wu, A. A. Talin, T. J. Udoovic, *Chem. Mater.* **2017**, *29*, 10496–10509.
- [30] D. H. P. Souza, A. M. D'Angelo, T. D. Humphries, C. E. Buckley, M. Paskevicius, *Dalton Trans.* **2022**, *51*, 13848–13857.
- [31] A. V. Skripov, G. Majer, O. A. Babanova, R. V. Skoryunov, A. V. Solonin, M. Dimitrievska, T. J. Udoovic, *J. Alloys Compd.* **2021**, *850*, 156781.
- [32] W. S. Tang, K. Yoshida, A. V. Solonin, R. V. Skoryunov, O. A. Babanova, A. V. Skripov, M. Dimitrievska, V. Stavila, S.-I. Orimo, T. J. Udoovic, *ACS Energy Lett.* **2016**, *1*, 659–664.
- [33] a) R. Asakura, D. Reber, L. Duchêne, S. Payandeh, A. Remhof, H. Hagemann, C. Battaglia, *Energy Environ. Sci.* **2020**, *13*, 5048–5058; b) M. Brighi, F. Murgia, Z. Łodziana, P. Schouwink, A. Wołczyk, R. Černý, *J. Power Sources* **2018**, *404*, 7–12.
- [34] L. Duchêne, R. S. Kühnel, E. Stilp, E. Cuervo Reyes, A. Remhof, H. Hagemann, C. Battaglia, *Energy Environ. Sci.* **2017**, *10*, 2609–2615.
- [35] M. Matsuo, S. Kuromoto, T. Sato, H. Oguchi, H. Takamura, S.-I. Orimo, *Appl. Phys. Lett.* **2012**, *100*, 203904.
- [36] L. He, H. Lin, H.-F. Li, Y. Filinchuk, J. Zhang, Y. Liu, M. Yang, Y. Hou, Y. Deng, H.-W. Li, H. Shao, L. Wang, Z. Lu, *J. Power Sources* **2018**, *396*, 574–579.
- [37] Y. Sadikin, P. Schouwink, M. Brighi, Z. Łodziana, R. Černý, *Inorg. Chem.* **2017**, *56*, 5006–5016.
- [38] B. R. S. Hansen, M. Paskevicius, M. Jørgensen, T. R. Jensen, *Chem. Mater.* **2017**, *29*, 3423–3430.
- [39] S. Li, P. Qiu, J. Kang, Y. Ma, Y. Zhang, Y. Yan, T. R. Jensen, Y. Guo, J. Zhang, X. Chen, *ACS Appl. Mater. Interfaces* **2021**, *13*, 17554–17564.
- [40] S. Li, P. Qiu, J.-X. Kang, Z. Shi, Y. Zhang, Y. Ma, X. Chen, *Mater. Chem. Front.* **2021**, *5*, 8037–8046.
- [41] M. Jørgensen, P. T. Shea, A. W. Tomich, J. B. Varley, M. Bercx, S. Lovera, R. Černý, W. Zhou, T. J. Udoovic, V. Stavila, *Chem. Mater.* **2020**, *32*, 1475–1487.
- [42] X. Luo, A. Rawal, C. Cazorla, K.-F. Aguey-Zinsou, *Adv. Sustainable Syst.* **2020**, *4*, 1900113.
- [43] a) Z. Yang, M. Jin, S. Cheng, X. Ma, Z. Qin, J. Zhang, Y. Yang, Y. Guo, *J. Mater. Chem. A* **2022**, *10*, 7186–7194; b) M. Jin, Z. Yang, S. Cheng, Y. Guo, *ACS Appl. Energ. Mater.* **2022**, *5*, 15578–15585; c) M. Jin, S. Cheng, Z. Yang, Y. Luo, Y. Guo, *Chem. Eng. J.* **2023**, *455*, 140904; d) M. Jin, D. Xu, Z. Su, Z. He, X. Chen, R. Wu, Y. Guo, *ACS Energy Lett.* **2024**, *9*, 1176–1183.
- [44] W. S. Tang, M. Matsuo, H. Wu, V. Stavila, A. Unemoto, S.-I. Orimo, T. J. Udoovic, *Energy Storage Mater.* **2016**, *4*, 79–83.
- [45] S. R. H. Jensen, M. Jørgensen, T. P. T. Nguyen, G. Nolan, C. E. Buckley, T. R. Jensen, M. Paskevicius, *Dalton Trans.* **2024**, *53*, 7619–7627.
- [46] a) E. L. Muettterties, J. H. Balthis, Y. T. Chia, W. H. Knoth, H. C. Miller, *Inorg. Chem.* **1964**, *3*, 444–451; b) L. He, H.-W. Li, E. Akiba, *Energies* **2015**, *8*, 12429–12438.
- [47] a) J. Aihara, *J. Am. Chem. Soc.* **1978**, *100*, 3339–3342; b) P. V. R. Schleyer, K. Najafian, *Inorg. Chem.* **1998**, *37*, 3454–3470.
- [48] M. P. Pitt, M. Paskevicius, D. H. Brown, D. A. Sheppard, C. E. Buckley, *J. Am. Chem. Soc.* **2013**, *135*, 6930–6941.
- [49] a) W. D. Richards, L. J. Miara, Y. Wang, J. C. Kim, G. Ceder, *Chem. Mater.* **2016**, *28*, 266–273; b) A. Unemoto, M. Matsuo, S.-I. Orimo, *Adv. Funct. Mater.* **2014**, *24*, 2267–2279.
- [50] C. A. Reed, *Acc. Chem. Res.* **1998**, *31*, 133–139.
- [51] R. N. Grimes, *Carboranes*, Academic Press **2016**.
- [52] M. Brighi, F. Murgia, R. Černý, *Cell Rep. Phys. Sci.* **2020**, *1*, 100217.
- [53] T. S. Kjær, J. B. Grinderslev, L. N. Skov, T. R. Jensen, *J. Mater. Chem. A* **2024**, *12*, 19485–19496.
- [54] K. Yoshida, T. Sato, A. Unemoto, M. Matsuo, T. Ikeshoji, T. J. Udoovic, S.-I. Orimo, *Appl. Phys. Lett.* **2017**, *110*, 103901.
- [55] M. Brighi, F. Murgia, R. Černý, *Adv. Mater. Interfaces* **2022**, *9*, 2101254.
- [56] R. Jiang, C. Song, J. Yang, J. Zhao, F. Fang, Y. Song, D. Sun, F. Wang, *Adv. Funct. Mater.* **2023**, *33*, 2301635.
- [57] F. Murgia, M. Brighi, R. Černý, *Electrochem. Commun.* **2019**, *106*, 106534.
- [58] L. Duchêne, D. H. Kim, Y. B. Song, S. Jun, R. Moury, A. Remhof, H. Hagemann, Y. S. Jung, C. Battaglia, *Energy Storage Mater.* **2020**, *26*, 543–549.
- [59] B. R. S. Hansen, M. Paskevicius, H.-W. Li, E. Akiba, T. R. Jensen, *Coord. Chem. Rev.* **2016**, *323*, 60–70.
- [60] C. Harzdorf, H. Niederprüm, H. Odenbach, *Z. Naturforsch. B* **1970**, *25*, 6–10.
- [61] a) L. He, H.-W. Li, S.-J. Hwang, E. Akiba, *J. Phys. Chem. C* **2014**, *118*, 6084–6089; b) L. He, H.-W. Li, H. Nakajima, N. Tumanov, Y. Filinchuk, S.-J. Hwang, M. Sharma, H. Hagemann, E. Akiba, *Chem. Mater.* **2015**, *27*, 5483–5486; c) L. He, Y. Fu, D. Wu, D. Zhang, H. Cheng, H. Lin, X. Li, W. Xiong, Q. Zhu, Y. Deng, H. Shao, H.-W. Li, X. Zhao, Z. Lu, *Inorg. Chim. Acta* **2018**, *474*, 16–21.
- [62] S. Li, Y. Zhang, Y. Ma, P. Qiu, X. Chen, *Organometallics* **2021**, *40*, 3480–3485.
- [63] H. Han, Y.-Y. Wang, X.-C. Yu, Y.-N. Ma, X. Chen, *Crystals* **2022**, *12*, 1399.
- [64] X.-M. Chen, N. Ma, Q.-F. Zhang, J. Wang, X. Feng, C. Wei, L.-S. Wang, J. Zhang, X. Chen, *J. Am. Chem. Soc.* **2018**, *140*, 6718–6726.
- [65] Y. Jing, X. Wang, H. Han, X.-R. Liu, X.-C. Yu, X.-M. Chen, D. Wei, L.-S. Wang, X. Chen, *Sci. China Chem.* **2024**, *67*, 876–881.
- [66] X.-M. Chen, X.-C. Yu, J.-X. Chi, Y. Jing, H. Wang, N. Zhang, C. Zhang, Y.-W. Ge, X. Chen, *Dalton Trans.* **2023**, *52*, 17684–17688.

Manuscript received: September 29, 2024

Revised manuscript received: November 5, 2024

Accepted manuscript online: November 22, 2024

Version of record online: December 1, 2024